b-more-incomplete and b-more-positive: Insights on A Robust Estimator of Magnitude Distribution

E. Lippiello[1] and G. Petrillo[2]

[1]Department of Mathematics and Physics, Universitá della Campania "L. Vanvitelli" , Viale Lincoln 5, 81100 Caserta, Italy

[2]The Institute of Statistical Mathematics, Research Organization of Information and Systems, Tokyo, Japan

Key Points:

- Conditional probability detecting consecutive earthquakes makes positive magnitude difference distribution weakly affected by incompleteness.
- The b-positive estimator can be enhanced by including more earthquake pairs, not only consecutive ones.
- The b-positive estimator can be enhanced by making the catalog more incomplete.

Corresponding author: E. Lippiello, `eugenio.lippiello@unicampania.it`

Abstract

The b-value in earthquake magnitude-frequency distribution quantifies the relative frequency of large versus small earthquakes. Monitoring its evolution could provide fundamental insights into temporal variations of stress on different fault patches. However, genuine b-value changes are often difficult to distinguish from artificial ones induced by temporal variations of the detection threshold. A highly innovative and effective solution to this issue has recently been proposed by van der Elst (2021) by means of the b-positive estimator, which is based on analyzing only the positive differences in magnitude between successive earthquakes.

Here, we demonstrate the robustness of the estimator, which remains largely unaffected by detection issues due to the properties of conditional probability. We illustrate that this robustness can be further improved by considering positive differences in magnitude, not only between successive earthquakes but also between different pairs of earthquakes. This generalized approach, defined as the "b-more-positive estimator," enhances efficiency by providing a precise estimate of the b-value while including a larger number of earthquakes from an incomplete catalog. However, our analysis reveals that the accuracy of the b estimators diminishes when earthquakes below the completeness threshold are included in the catalog. This leads to the paradoxical observation that greater efficiency is achieved when the catalog is more incomplete. To address this, we introduce the "b-more-incomplete estimator", where the b-more-positive estimator is applied only after artificially filtering the instrumental catalog to make it more incomplete. Our findings show the superior efficiency of the b-more-incomplete method.

Plain Language Summary

Earthquake magnitudes can vary widely, and the b-value is a common metric used to measure the frequency of earthquakes with large versus small magnitudes. In addition, the b-value could serve as an indicator of the stress state of different fault patches, making it a valuable tool in earthquake research. However, since small earthquakes are often obscured by previous larger ones, determining whether changes in the b-value are genuine or simply caused by detection problems can be challenging. To address this issue, a new approach called the b-positive estimator has been recently developed. The method only considers positive changes in magnitude between successive earthquakes.

In this study, we confirm that the b-positive estimator is a powerful and effective technique to estimate the b-value and is largely unaffected by issues related to detecting earthquakes. We extend the method by considering positive differences in magnitude, encompassing not only successive earthquakes but also different pairs of earthquakes. In particular we show that because of the puzzling aspects of conditional probabilities, the b-positive estimator is more efficient when the catalog is more incomplete. This allows us to develop modifications to the b-positive method providing a more efficient tool to monitor the b-value in ongoing seismic sequences.

1 Introduction

The Gutenberg and Richter (GR) law (Gutenberg & Richter, 1944) provides a good description of the probability $p(m)$ of observing an earthquake of magnitude m, with $p(m)$ given by

$$p(m) = b \ln(10) 10^{-b(m-m_L)}, \tag{1}$$

where b is the scaling parameter and m_L is a lower bound for the magnitude. The hypothesis that the b-value is correlated with the stress state (Scholz, 1968; Wyss, 1973; Amitrano, 2003; Gulia & Wiemer, 2010; Scholz, 2015) has spurred investigations into detecting spatio-temporal variations in b-value, which could serve as indicators of stress changes triggered by significant foreshocks and precursor patterns (Wiemer & Wyss, 1997, 2002; Gulia & Wiemer, 2010; Nanjo et al., 2012; Tormann et al., 2014, 2015; Gulia & Wiemer, 2019; Gulia et al., 2020; Nanjo, 2020). The decrease of the b-value during foreshock activity has been explained in terms of stress relaxation and accumulation in mechanical models for the seismic fault (Lippiello, Petrillo, Landes, & Rosso, 2019; Petrillo et al., 2020). On the other hand, accurately differentiating between genuine and spurious variations in instrumental catalogs, continues to pose a significant challenge (Marzocchi et al., 2019). This is because the detection threshold presents irregular behavior and small earthquakes can go unreported due to inadequate spatial coverage of the seismic network (Schorlemmer & Woessner, 2008; Mignan et al., 2011; Mignan & Woessner, 2012) or being obscured by coda waves generated by previous larger earthquakes (Kagan, 2004; Helmstetter et al., 2006; Peng et al., 2007; Lippiello et al., 2016; Hainzl, 2016a, 2016b; de Arcangelis et al., 2018; Petrillo et al., 2020; Hainzl, 2021). Failure to properly account for both mechanisms can lead to a significant underestimation of the b-value. To address the issue of incomplete reporting, a common approach is to limit the evaluation of the

b-value to magnitudes greater than a threshold M_{th}. This threshold is typically chosen to be larger than the completeness magnitude M_c, which is defined as the magnitude above which detection are not impacted by completeness issues. However, the constraint on magnitudes $m > M_{th}$ can pose challenges for monitoring spatio-temporal variations in the b-value since it necessitates using a restricted number N of earthquakes within each space-time region. While the finite value of N can be accommodated to correct for systematic positive biases in the b-value (Godano et al., 2023), it also introduces statistical fluctuations (Shi & Bolt, 1982) that, for small data sets, can become significant and mask genuine b-value variations.

A remarkably innovative solution to the problem has been recently proposed by van der Elst (2021). He introduced the "b-positive" estimator, which obtains the b-value from the distribution of magnitude differences $\delta m = m_{i+1} - m_i$ between two consecutive earthquakes i and $i+1$ in the catalog. In particular, for a complete data set that obeys the GR law (Eq.1), it is easy to show that the distribution of δm, $p(\delta m)$, is an exponential function with exactly the same coefficient $b_+ = b$. The striking result by van der Elst (2021), corroborated by extended numerical simulations, is that if one restricts to positive δm, $p(\delta m)$ is much less affected by detection problems than $p(m)$, and $b_+ \simeq b$ also for incomplete catalogs.

A simple explanation for the effectiveness of the b-positive estimator is that by restricting to positive values of δm, the method focuses on larger magnitude earthquakes that are less affected by detection thresholds or limitations. However, at first glance, this approach may not seem significantly different from imposing the condition $m > M_{th}$ on $p(m)$, and it does not reveal the unique advantages of the b-positive estimator.

In our manuscript, we shed light on the deeper implications of constraining $m_{i+1} > m_i$ in the presence of detection issues. We demonstrate how the properties of conditional probabilities reveal the exceptional efficiency of the b-positive estimator. Indeed we will show that even for extremely incomplete catalogs, under specific conditions, the b-positive estimator provides an exact and precise measure of the b-value. This occurs also when its standard estimate via the GR law requires such a large value of M_{th} that it is dominated by statistical fluctuations.

In particular, the relationship $b_+ = b$ holds exactly under the assumption that only events above the completeness level M_c are reported in the catalogs. However, in instrumental catalogs, it is reasonable to assume that a fraction of earthquakes with magnitudes $m_i < M_c$ are identified. This introduces biases in the b-positive estimator. Nevertheless, such conditions occur infrequently, rendering b_+ consistently a very good approximation for the true b-value. After identifying the mechanisms responsible for the accuracy of the b-positive estimator, we also propose various generalizations to further improve the efficiency of b-value estimates through the analysis of the magnitude difference distribution. Here, efficiency refers to the possibility of a precise estimation of the b-value, achieved by utilizing the largest subset N of earthquakes from the catalog. It's important to note that as we increase N, the associated uncertainty δb in our b estimate decreases. Therefore, the most efficient estimator is the one that provides the correct b-value with the smallest uncertainty, i.e., utilizing the largest value of N.

2 Magnitude incompleteness

Incomplete earthquake catalogs result from two primary factors: seismic network density incompleteness (SNDI) and short-term aftershock incompleteness (STAI). SNDI occurs when earthquakes are challenging to detect due to a low signal-to-noise ratio. Several factors, including noise filtering capabilities and the distance between earthquake epicenters and the necessary seismic stations for locating an event, can contribute to SNDI (Mignan & Woessner, 2012). Conversely, STAI arises from detection issues in the aftermath of large earthquakes, primarily caused by the masking effect of small aftershocks obscured by coda waves from previous larger ones (Lippiello, Petrillo, Godano, et al., 2019). A more detailed description of SNDI and STAI can be found in Appendix A.

SNDI and STAI, combined, lead to a completeness magnitude $M_c(t_i, \vec{x_i}, \mathcal{H}_i)$, which depends on the the occurrence time t_i, epicenter coordinates $\vec{x_i}$, and the past seismic history $\mathcal{H}_i$, encompassing all prior earthquakes up to time t_i. We assume that all earthquakes with a magnitude greater than M_c are reported in the catalog. Simultaneously, various factors such as diurnal and seasonal variations, changes in staffing, etc., can introduce fluctuations of approximately σ in the completeness level. Considering these fluctuations, the probability that an earthquake with magnitude m, occurring at time t and location $\vec{x}$, is reported in the catalog, is described by the detection function $\Phi(m - M_c)$, given by:

$$\Phi(m - M_c) = \begin{cases} 1 & \text{if } m - M_c > 0 \\ 1 + \text{Erf}\left(\frac{m-M_c}{\sigma}\right) & \text{if } m - M_c \leq 0 \end{cases} \tag{2}$$

Here, $\text{Erf}(y)$ represents the error function. According to this definition, all earthquakes with $m > M_c$ are reported in the catalog, while only about 2% of earthquakes with $m < M_c - 2\sigma$ are included. The typical behavior of $\Phi(y)$ for different σ values is illustrated in Fig. (1).

It's important to note that the detection function $\Phi(y)$ (Eq. (2)) slightly differs from the one proposed in (Ogata & Katsura, 1993), which assumes $\Phi(m-M_c) = \frac{1}{2}+\frac{1}{2}\text{Erf}\left(\frac{m-M_c}{\sigma}\right)$, indicating that, on average, only 50% of earthquakes with $m > M_c$ are reported in the catalog. Both definitions coincide in the limit case where $\sigma \to 0$.

3 Analytical results

We denote by $p(m_i, t_i, \vec{x}_i)$ the probability of observing an earthquake with magnitude m_i at time t_i and location $\vec{x}_i$. For a complete dataset, it is reasonable to assume that magnitudes follow the Gutenberg-Richter (GR) law given by Eq. (1), independently of the occurrence time and location. Under this assumption, $p(m_i, t_i, \vec{x}_i)$ takes the form

$$p(m_i, t_i, \vec{x}_i) = \beta e^{-\beta(m_i - m_L)} \Lambda(t_i, \vec{x}_i \,|\, \mathcal{H}_i), \tag{3}$$

where $\beta = b \log(10)$, and $\Lambda(t_i, \vec{x}_i \,|\, \mathcal{H}_i)$ is the probability density of having an earthquake at time t_i and location $\vec{x}_i$. We explicitly mention that Λ depends on the seismic history $\mathcal{H}_i$ up to time t_i. By definition, the integral of Λ over the entire region and time window is normalized to 1.

Correlations with previous seismicity are caused (Lippiello et al., 2007, 2012) by the detection problems discussed in the previous Sec.2. This implies that

$$p\left(m_i, t_i, \vec{x}_i\right) = \beta e^{-\beta(m_i - m_L)} \Lambda\left(t_i, \vec{x}_i | \mathcal{H}_i\right) \Phi\left(m_i - M_c\left(t_i, \vec{x}_i, \mathcal{H}_i\right)\right). \tag{4}$$

3.1 Traditional estimator of the *b*-value

The standard method for evaluating the b-value in the presence of incompleteness involves restricting the analysis to magnitudes greater than a threshold value M_{th}. This

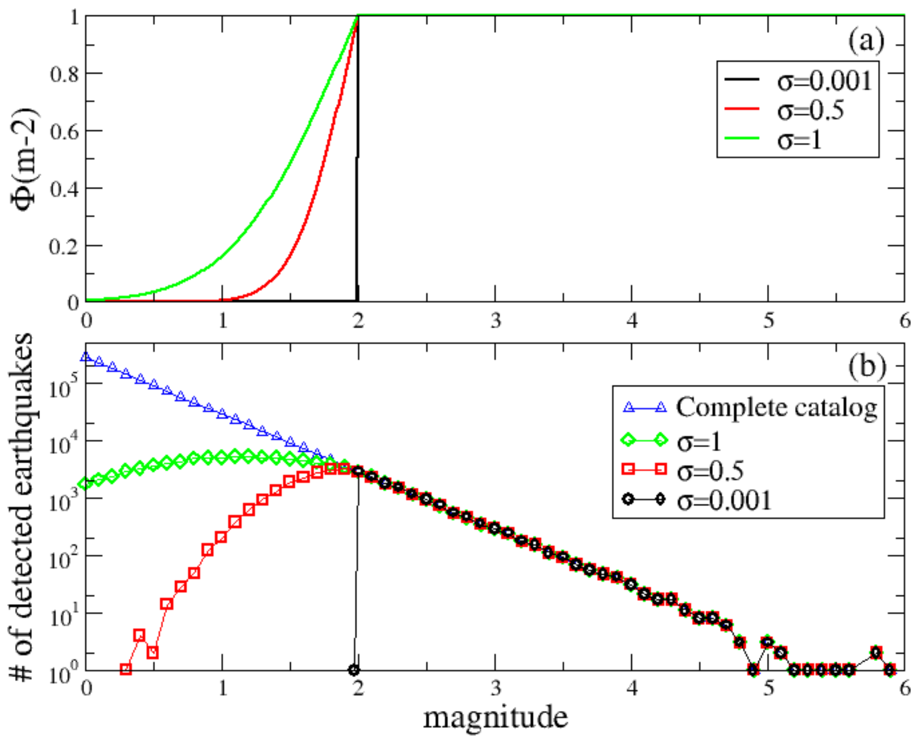

Figure 1. (Color online) (a) The detection function $\Phi(m - M_c)$, with $M_c = 2$, for three values of σ: 0.001, 0.5, and 1 (see legend). (b) The impact of the detection function $\Phi(m - M_c)$ on the magnitude distribution within a simulated catalog comprising 1.3×10^6 earthquakes with $m > 0$, following a GR distribution with $b = 1$. In the plots, blue triangles represent the magnitude distribution for the complete dataset, while different colors and symbols are used for the magnitude distribution in the incomplete catalog for varying σ values (refer to the legend for details).

threshold should be chosen sufficiently large to satisfy the condition $M_{th} > M_c$ and therefore

$$\Phi\left(M_{th} - M_c(t_i, \vec{x}_i, \mathcal{H}_i)\right) = 1. \tag{5}$$

In this case, the probability of observing an earthquake with magnitude m_i can be obtained from Eq.(3) after integrating over space and time, and it is given by $\beta e^{-\beta(m_i - m_{th})}$. Through likelihood maximization, we ultimately determine the b-value (Aki, 1965):

$$b(M_{th}) = \frac{1}{\ln(10)(\langle m \rangle - M_{th})}, \tag{6}$$

where $\langle m \rangle$ represents the average magnitude in the dataset containing N earthquakes with $m > M_{th}$.

However, as explained in Sec. 2, M_c varies in both time and space. Therefore, Eq. (5) holds true only if M_{th} coincides with the maximum value of M_c within the considered space-time region. Consequently, one is compelled to choose large values for M_{th}, but this poses a challenge. A too-large value of M_{th} results in a smaller number N of earthquakes used in the evaluation (Eq. (6)), leading to a larger uncertainty δb in the estimation of the b-value. This is why this strategy is inefficient, especially when dealing with the early stages of aftershock sequences, where M_c exhibits large values due to STAI.

We further observe that Eq.(6) holds in the hypothesis that magnitudes are continuous random variables. However, in earthquake catalogs, magnitudes are often reported only to one or two decimal places. In such cases, a correcting term needs to be added to the denominator of Eq.(6) to account for this discretization. Alternatively, as suggested by Godano et al. (2014), we can add a random noise term to the last digit of the reported magnitudes to make them continuous, and then apply Eq.(6). In the following analysis, we will adopt this strategy.

3.2 Probability distribution $p(\delta M)$ in complete data sets

We consider the probability $p(m_j, t_j, \vec{x}_j | m_i, t_i, \vec{x}_i)$ to observe an earthquakes m_j at time t_j in the position $\vec{x}_j$ conditioned to the occurrence of a previous earthquake with magnitude m_i occurred at the previous time $t_i < t_j$ in the position $\vec{x}_i$. In the hypothesis of a complete data set with occurrence probability given by Eq.(3), the occurrence of the magnitude m_j is uncorrelated to what happens at previous times. In this case

$$p(m_j, t_j, \vec{x}_j | m_i, t_i, \vec{x}_i) = \beta e^{-\beta(m_j - m_L)} \Lambda\left(t_j, \vec{x}_j | \mathcal{H}_j\right), \tag{7}$$

and it is easy to show (see Appendix B) that the probability density $p(\delta m)$ to have $m_j = m_i + \delta m$ is given by

$$p(\delta m) = \frac{1}{2} \beta e^{-\beta \delta m}, \tag{8}$$

which is a well known result for the distribution of the difference of two independent random variables with identical exponential distributions. Eq.(8) shows that, in the ideal case, δm follows an exponential law equivalent to the GR law with exactly the same coefficient β. In the following, we define b_+ as the b-value obtained from $p(\delta m)$, restricting it to $\delta m > 0$. Through likelihood maximization, we obtain from Eq. (8):

$$b_+ = \frac{1}{\ln(10)} \frac{1}{\langle \delta m \rangle}, \tag{9}$$

which gives $b_+ = b$ in a fully complete catalog.

We observe the importance of the factor 1/2 in Eq.(8), indicating that the condition $\delta m > 0$ is met, on average, by only half of the earthquakes in our dataset. Specifically, in the b-positive estimator, we set $j = i+1$, which means we're considering only earthquakes that are followed by a larger one. These earthquakes make up approximately 50% of the dataset. In the ideal case of a complete dataset, therefore, the estimate of the b-value from Eq.(9), defined "b-positive" estimator, is less efficient than the traditional estimator from Eq.(6), as the latter uses the entire dataset.

We can enhance the efficiency of the b-positive estimator by systematically exploring, in increasing order, all possible j values within the range $j \in [i+1, i+l]$, where $l \geq 1$. We continue this exploration until we reach a value of j where $m_j \geq m_i$. In this case, the probability distribution for finding $m_j = m_i + \delta m$, with $\delta m > 0$, is given by:

$$p_l(\delta m) = K_l \beta e^{-\beta \delta m}, \ \delta m > 0 \tag{10}$$

with $K_l = \frac{l}{l+1}$ (Eq.B3). It's clear that K_l approaches 1 for sufficiently large l, signifying the inclusion of all earthquakes from the original dataset in the computation of the b-value. From the maximization of likelihood, this procedure defined "b-more-positive" estimator, ultimately leads to an estimate for the b-value:

$$b_{+l} = \frac{1}{\ln(10)} \frac{1}{\langle \delta m \rangle_l}. \tag{11}$$

This differs from Eq. (9) due to the fact that $\langle \delta m \rangle_l$ in Eq. (11) represents the average magnitude difference between $\delta m = m_j - m_i$, where $j \in [i+1, i+l]$ is the index of the first earthquake recorded after i, with $m_j > m_i$. In other words, all earthquakes with an index in the range $[i{+}1, j{-}1]$ have a magnitude smaller than m_i. Conversely, in Eq. (9), $\langle \delta m \rangle$ is the average difference between m_{i+1} and m_i and is only evaluated in cases where $m_{i+1} > m_i$.

Therefore, in the b-positive estimator, only half of the dataset is used to evaluate b_+, whereas in the b-more-positive estimator, for sufficiently large l, the evaluation of b_{+l} includes a much higher percentage of the dataset, which significantly reduces the uncertainty δb. Obviously, the b-positive estimator is a special case of the b-more-positive estimator, specifically when $l = 1$. Consequently, in the subsequent discussion, we will focus on the b-more-positive estimator, while bearing in mind that the findings also apply to the b-positive estimator under the condition $l = 1$.

3.3 Probability distribution $p(\delta M)$ in incomplete data sets

In the case of an incomplete dataset, Eq. (7) must be replaced by:

$$p(m_j, t_j, \vec{x}_j \,|\, m_i, t_i, \vec{x}_i) = \beta e^{-\beta(m_j - m_L)} \Lambda(t_j, \vec{x}_j) \Phi\left(m_j - M_c(t_j, \vec{x}_j, \mathcal{H}_j | m_i)\right). \qquad (12)$$

Here, we explicitly use the notation $\Phi\left(m_j - M_c | m_i\right)$ to specify that the detection function must be evaluated under the condition that the previous earthquake m_i has been identified and reported in the catalog. This information is crucial for the efficient evaluation of the b-value. It is easy to show (Appendix B) that when the condition

$$\Phi\left(m_j - M_c(t_j, \vec{x}_j, \mathcal{H}_j \,|\, m_i)\right) = 1 \qquad (13)$$

is satisfied in Eq. (12), we obtain

$$p(\delta m) = \beta e^{-\beta \delta m} K, \qquad (14)$$

where K is a constant whose expression can be found in Appendix B. Eq. (14) shows that the dependence of $p(\delta m)$ on δm is an exponential function with a coefficient β that is not affected by incompleteness and exactly coincides with $b \ln(10)$. Therefore, when condition Eq. (13) holds, Eq. (11) provides the exact b-value, even in the presence of incompleteness. Detection problems only affect the value of K, which depends on $\Phi(m_i - M_c(t_i, \vec{x}_i, \mathcal{H}_i))$ (Eq. (B5)).

We want to emphasize that the information regarding the previous earthquake with magnitude m_i has been recorded and reported in the catalog significantly simplifies the satisfaction of condition (13), as compared to condition (5) whose validity is necessary for the accuracy of the traditional estimator. More precisely, two hypotheses are sufficient to ensure the validity of condition (13):

- Hypothesis i): $M_c(t_j, \vec{x}_j, \mathcal{H}_j) \leq M_c(t_i, \vec{x}_i, \mathcal{H}_i)$.
- Hypothesis ii): $\sigma \to 0$.

Let us indeed assume that hypothesis ii) holds. In this case, the information that m_i has been recorded and is present in the dataset automatically implies that $m_i > M_c(t_i, \vec{x}_i, \mathcal{H}_i)$. Accordingly, since $m_j > m_i$, the validity of hypothesis i) automatically implies $m_j > M_c(t_j, \vec{x}_j, \mathcal{H}_j)$, and therefore the condition (13) is satisfied. Therefore, if the two hypotheses are satisfied, the condition $m_j > m_i$ is sufficient to exclude the possibility of the existence of earthquakes larger than m_i occurring in the time interval $[t_i, t_j]$ and not reported in the catalog. As a consequence, for each earthquake m_i reported in the catalog, the magnitude difference $\delta m = m_j - m_i$ would be exactly the same as what we would have measured in a complete catalog, and b_{+l} obtained from Eq. (11) coincide with the true b-value. The only difference with the distribution of the magnitude difference evaluated in the complete catalog (Eq.(10)) being in the constant K being smaller than K_l. In particular, when $l \gg 1$ and $K_l \to 1$, the estimation of b through b_{+l} employs the entirety of the earthquakes which have been recorded in the instrumental catalog. In contrast, the estimation achieved using $b(M_{th})$ only takes into account earthquakes with a magnitude exceeding M_{th}, which, especially for significantly large M_{th} values, can be a minute portion of N_{cat}. This essential distinction is what renders the b-more-positive estimator notably more efficient than the traditional estimator.

It's crucial to emphasize that this scenario holds valid solely when both hypotheses i) and ii) are satisfied. In the forthcoming section, we explore the prerequisites for their applicability in instrumental datasets.

3.4 Conditions for the validity of the two hypotheses

The effectiveness of the b-positive method is proven when the two hypotheses i) and ii) hold. Here we discuss how to construct circumstances for their realization by taking into account the two mechanisms SNDI and STAI responsible for incompleteness (Sec. 2).

3.4.1 The validity of hypothesis i)

It is easy to create conditions such as hypothesis i) holds. Indeed, if we assume that the epicentral distance d_{ij} between the two earthquakes is sufficiently small it becomes reasonable that the two earthquakes occur in regions with a similar network coverage such as $M_c(t_i, \vec{x}_j, \mathcal{H}_i) = M_c(t_i, \vec{x}_i, \mathcal{H}_i)$, i.e. incompleteness at the same time in the two positions $\vec{x}_i$ and $\vec{x}_j$ coincide. Furthermore, we must take into account that in the b-more-positive estimator, j is the first larger earthquake recorded after the earthquake i and there is no intermediate earthquake occurred in the time interval $[t_i, t_j]$ responsible for obscuration effects on the earthquake with magnitude $m_j > m_i$. According to STAI, M_c decreases over time and therefore, the completeness magnitude at the subsequent time $t_j > t_i$ is smaller than $M_c(t_i, \vec{x}_i, \mathcal{H}_i)$ and hypothesis i) is fulfilled. Accordingly, hypothesis i) can be imposed by setting $d_{ij} < d_R$, where d_R is a sufficient small distance and selecting m_j as the first earthquake larger than m_i present in the catalog and with a distance d_{ij} smaller than d_R.

We would like to point out that the condition $d_{ij} < d_R$ was not taken into consideration by van der Elst (2021). However, it is important to emphasize that when focusing on evaluating the b-value within a seismic sequence, the criteria chosen for selecting aftershocks typically limit them to a smaller region surrounding the mainshock. Under these circumstances, the aftershocks are closely clustered, occurring in areas with very similar network coverage, and the condition $d_{ij} < d_R$ is inherently met.

3.4.2 The validity of hypothesis ii)

In the subsequent discussion, we assume that the condition $d_{ij} < d_R$ is imposed to satisfy hypothesis i). However, even in this scenario, the presence of $\sigma \neq 0$ in Eq.(2) can invalidate the condition (13). Specifically, when both m_i and m_j fall within the magnitude range $(M_c - 2\sigma, M_c)$, there exists a finite probability, despite $m_j > m_i$ and hypothesis i) being satisfied, that m_i is recorded in the catalog while m_j is not. Consequently, $\Phi\left(m_j - M_c(t_j, \vec{x}_j, \mathcal{H}_j)\right) < 1$, rendering condition 13 invalid.

To ensure the validity of condition (13) one potential strategy is to restrict the values of m_j to be greater than $m_i+\delta M_{th}$, with $\delta M_{th} \gtrsim 2\sigma$. In this scenario, even when $m_i \in (M_c - 2\sigma, M_c)$ has a finite likelihood of being detected, $m_j > M_c$ guarantees a probability of 1 for detection, thereby preserving the validity of Eq.(13). For a finite δM_{th}, Eq.(9) must be adapted to yield:

$$b_+(\delta M_{th}) = \frac{1}{\ln(10)} \frac{1}{\langle \delta m \rangle - \delta M_{th}}, \tag{15}$$

This approach converges to the true b-value for $\delta M_{th} \gtrsim 2\sigma$. However, determining the value of σ from data is challenging. To identify the optimal δM_{th}, one can seek the minimum value where $b_+(\delta M_{th})$ no longer depends on δM_{th}, a strategy proposed by van der Elst (2021).

We can also extend Eq.(11) to account for a finite σ

$$b_{+l}(\delta M_{th}) = \frac{1}{\ln(10)} \frac{1}{\langle \delta m \rangle_l - \delta M_{th}}, \tag{16}$$

Here, $\langle \delta m \rangle_l$ denotes the average magnitude difference for $\delta m = m_{i+l} - m_i$, where $l \geq 1$, and $m_k \leq m_i$ for $k \in [i+1, j)$ and $m_j \geq m_i + \delta M_{th}$. It's important to note that requiring $m_k \leq m_i + \delta M_{th}$ for $k \in [i+1, i+l-1]$, as opposed to just $m_k \leq m_i$, leads to an erroneous estimate of the b-value through Eq.(16).

In the following we propose an alternative two-step strategy referred to as "b-more-incomplete" estimator. The first step corresponds to filter the catalog by removing all earthquakes with magnitudes below a threshold M_A. In particular we employ a filtering approach where earthquakes occurring within a temporal distance less than τ after a previous larger earthquake are removed from the catalog. This corresponds to a constant blind time $\tau = \delta t_0$ (Hainzl, 2016b, 2016a, 2021) and a threshold magnitude $M_A\left(t_i, \vec{x}_i, \mathcal{H}_i\right) = M_T\left(t_i, \vec{x}_i, \mathcal{H}_i\right)$ as defined in Eq.(A3) with the functional form Eq.(A4) for M_t. In the second step the b-more-positive estimator is applied to the filtered catalog. The crucial factor lies in our ability to fine-tune M_A such that $M_A \gtrsim M_c$. When achieved, the filtered catalog will exhibit a detection function with $\sigma = 0$, and hypothesis ii) will be realized. We denote the b-value derived from Eq. (11) using the average value of $\langle \delta m \rangle_l$ after applying the filter with a blind time τ to the catalog as $b_+^f(\tau)$. Since this filter results in a more incomplete catalog, we aptly refer to this estimator as the "b-more-incomplete" estimator. It's important to note that this estimator yields an accurate estimate of the b-value only when we select an M_A that closely aligns with M_c. Specifically, it's essential to configure the blind time τ such that $\tau \gtrsim \tau_{exp}$, where τ_{exp} represents the blind time typically observed in instrumental catalogs. However, since τ_{exp} is challenging to determine from data, the optimal approach involves evaluating $b_+^f(\tau)$ for increasing values of τ and stopping when it no longer depends on τ. We remark that the b-more-incomplete estimator can only reduce detection problems caused by STAI but it is not relevant to take into account SNDI.

4 Comparison of the different strategies to estimate the b-value

4.1 Pictorial description of the different methods

In Fig.2 we illustrate the different methods by considering an example of a seismic sequence which follows a magnitude $m = 6$ mainshock. In the considered example 8 $m > 3$ aftershocks have occurred during the first minute after the mainshock. In Fig.2a we consider the case of a complete data set where all the occurred earthquakes are reported in the catalog. Continuous black arrows are used to connect earthquake pairs which are included in the evaluation of the b-value in the b-positive method. The b-more-positive method includes in the evaluation also the pairs connected by magenta dot-dashed arrows. It is evident that the b-more-positive method uses more information from the same data set, providing a more efficient method for the b value evaluation. In Fig.2b we consider the case of an incomplete data set in the case $\sigma = 0$. In this example all the earthquakes below M_c, represented by the dashed green line, are not reported in the catalog. The b-positive method considers only the magnitude difference between earthquakes 4 and 7 (continuous black arrow), whereas the b-more-positive method also includes the magnitude difference between earthquakes 1 and 7 (magenta dot-dashed arrow). The comparison betwenn panels (a) and (b) illustrates that the b-more-positive method includes in the evaluation the same earthquakes pairs for both a complete and an incomplete data set. The only difference is the number of considered pairs being much smaller for the incomplete catalog. In Fig.2c we finally consider the case of an incomplete data set with a finite σ value. In this case the dotted red line represents $M_c - 2\sigma$ and earthquakes occurred between the dashed green line and the dotted red line have a finite probability to be recorded. In the specific example, earthquakes 2 and 5 have been recorded whereas earthquake 3 and 6 are not reported in the catalog. In this example the b-positive method considers the magnitude difference between earthquakes 2 and 4 and between earthquakes 5 and 7 (orange dot-dashed lines). It is evident that the two magnitude differences are larger than the one which one would have included in the complete data set (Fig.2a). This leads to a systematically smaller b value obtained from Eq.(9). In order to avoid this bias one can impose that the magnitude difference $m_{i+1}-m_i$ should be larger than δM_{th}. In the specific example setting $\delta M_{th} = 0.2$ also in the complete data set (Fig.2a) the b-positive method would consider the magnitude difference between earthquakes 2 and 4 and between earthquakes 5 and 7 (orange dot-dashed lines) which are exactly the same considered in Fig.2c. The bias in the estimate of the b value from Eq.(9) is then corrected by the presence of a finite δM_{th} in the denominator of Eq.(15). As an alternative strategy, in the b-more-incomplete method we remove from the catalog all the earthquakes below the threshold M_A, indicated as a blue dot-dot-dashed line in Fig.2b. In this example earthquakes 3 and 6 are removed from the filtered catalog and the b-more-positive method only includes the earthquake pairs considered in the case $\sigma = 0$ and which provides an exact estimate of the b-value.

4.2 Numerical analysis

In the previous section we have reported four strategies to evaluate the b-value. The traditional estimator is based on the measure of $b(m_{th})$ from Eq.(6), the b-positive estimator proposed by van der Elst (2021) based on the quantity $b_+(\delta M_{th})$ defined in Eq.(15), the b-more-positive estimator based on the quantity $b_{+l}(\delta M_{th})$ defined in Eq.(16) and finally the b-more-incomplete estimator based on the quantity $b_+^f(\tau)$. In the evaluation of the last two estimators we take the parameter $l = 10$. Indeed, the computation time for their evaluation grows proportionally to l, and therefore $l = 10$ represents a compromise for a sufficient large value of $K_l > 0.9$ (Eq.(B11) while keeping a sufficiently short computational time. By keeping l fixed, all the estimators present one tuning parameter, M_{th}, for the standard method, δM_{th} for the b-positive and the b-more-positive estimators and τ, for the b-more-incomplete estimator. In all cases, for sufficiently large values of the tuning parameter each of the four methods will converge to the exact b-value.

In the following sections we compare the four strategies via extended numerical simulations.

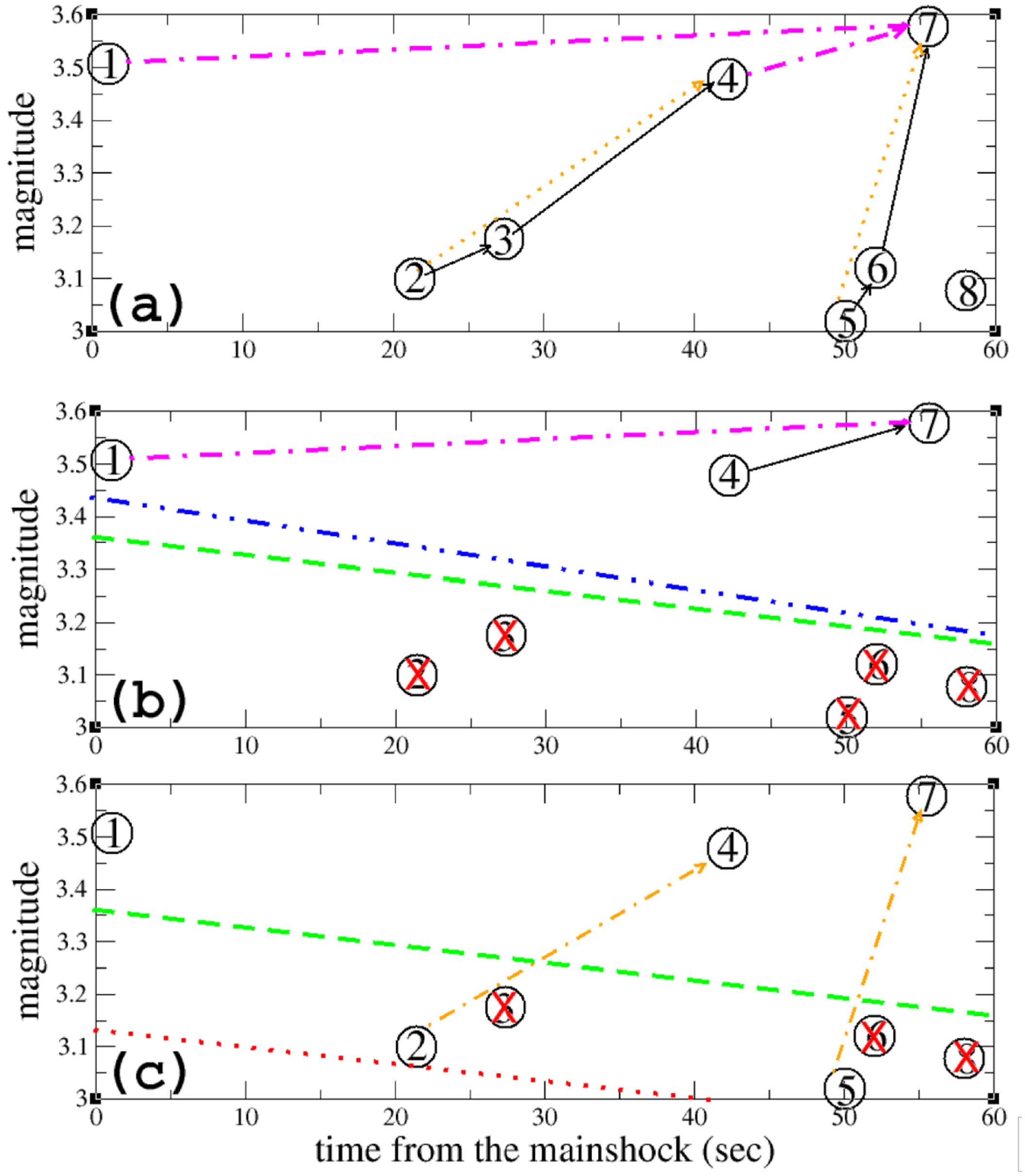

Figure 2. An illustration of a seismic sequence following a magnitude 6 mainshock. Aftershocks are labeled based on their occurrence time following the mainshock. (Panel a) Continuous black arrows connect earthquake pairs considered in the b-positive estimator. The b-more-positive estimator includes these pairs as well as those connected by dot-dashed magenta arrows. Dotted orange arrows connect earthquake pairs with a magnitude difference $m_j - m_i > \delta M_{th} = 0.2$. (Panel b) The green dashed line represents the completeness level $M_c(t_j, \vec{x}_j, \mathcal{H}_j)$. In this example, $\sigma = 0$, and all earthquakes with magnitudes smaller than M_c are not included in the catalog. The black continuous arrow is retained to connect the sole earthquake pair considered in the b-positive estimator, whereas the magenta dot-dashed arrow links another earthquake pair which is also taken into account in the b-more-positive estimator. The blue dot-dot-dashed line represents M_A, delineating that only earthquakes with $m > M_A$ are encompassed within the b-more-incomplete estimator. (Panel c) The green dashed line still represents the completeness level $M_c(t_j, \vec{x}_j, \mathcal{H}_j)$, the red dashed line corresponds to $M_c - 2\sigma$. Dotted orange arrows connect earthquake pairs used in the b-positive estimator.

5 Numerical simulations

We generate synthetic earthquake catalogs to simulate two distinct scenarios. In the first scenario, we simulate a single Omori sequence using the ETAS model (Ogata, 1985, 1988b, 1988a, 1989) with a single Poisson event, which is the initial event in the sequence. We assume that this first event occurs at time $t = 0$ with epicentral coordinates $(0, 0)$ and magnitude $m_1 = 8$. We employ a standard algorithm to simulate the cascading process (de Arcangelis et al., 2016) with realistic parameters obtained through likelihood maximization in Southern California (Bottiglieri et al., 2011). We verify the robustness of the results across different parameter choices. In the second scenario, we generate a complementary catalog that exclusively contains background earthquakes. These earthquakes follow a Poisson distribution in time, while their spatial distribution conforms to the background occurrence rate estimated by Petrillo and Lippiello (2020) for the Southern California region.

In both catalogs, we assume that earthquakes obey the GR law with a theoretical b-value of $b_{true} = 1$. It's worth noting that equivalent results are obtained for other selections of b_{true}. Starting from an initially complete catalog up to the lower magnitude threshold $m_L = 1$, we systematically remove events from the catalogs based on the detection function Φ described in Sec.2. We then estimate various quantities from these incomplete catalogs, including $b(M_{th})$ (Eq.(6)), $b_+(\delta M_{th})$ (Eq.(15)), $b_{+l}(\delta M_{th})$ (Eq.(16)), and $b_+(\tau)$ as defined in Sec.3.3. In both scenarios, we explore different levels of incompleteness, tuned by changing the value of σ in the detection function $\Phi(m-M_c)$ (Eq.(2). For each set of model parameters assigned, we consider $n_{\mathrm{real}} = 100$ different synthetic catalogs, each obtained using a different seed in the random number generator implemented in the numerical code. Then, we estimate the mean value of the aforementioned quantities and their standard deviation by averaging over the different catalogs. As an example, when evaluating $b(M_{\mathrm{th}})$, we consider the mean value $\langle b(M_{\mathrm{th}})\rangle = \frac{1}{n_{\mathrm{real}}}\sum_{n=1}^{n_{\mathrm{real}}} b_n(M_{\mathrm{th}})$ and the standard deviation $\delta b(M_{\mathrm{th}}) = \sqrt{\frac{1}{n_{\mathrm{real}}}\sum_{n=1}^{n_{\mathrm{real}}} \left(b_n(M_{\mathrm{th}}) - \langle b(M_{\mathrm{th}})\rangle\right)^2}$, where $b_n(M_{\mathrm{th}})$ represents the value of $b(M_{\mathrm{th}})$ estimated from Eq. (6) for the n-th synthetic catalog. For each value of M_{th}, we also evaluate the average value $\langle N\rangle = \frac{1}{n_{\mathrm{real}}}\sum_{n=1}^{n_{\mathrm{real}}} N_n$ with N_n being the number of earthquakes with $m > M_{\mathrm{th}}$ in the n-th catalog. Equivalent definitions are applied to evaluate the average values of $b_+(\delta M_{\mathrm{th}})$, $b_{+l}(\delta M_{\mathrm{th}})$, and $b_+(\tau)$, along with their associated standard deviations. For the sake of clarity, N_n corresponds to the number of earthquake pairs in the n-th synthetic catalog, with $m_{i+1} \geq m_i + \delta M_{\mathrm{th}}$

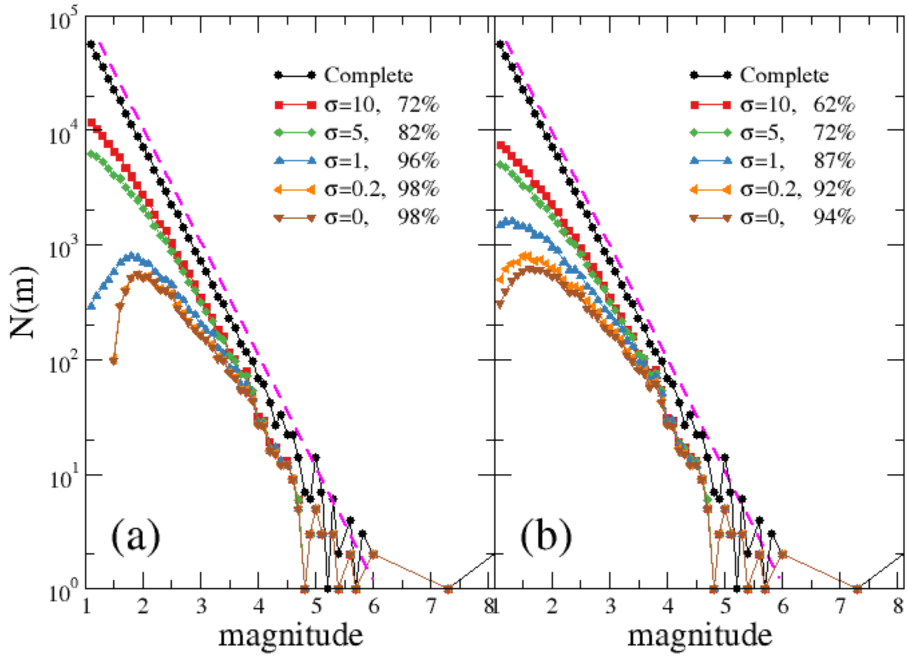

Figure 3. (Color online) The number of earthquakes $N(m)$ with magnitude in $[m, m + 1)$ in the numerical catalog with STAI implemented via the detection function Φ with two different choices of $M_t(t - t_i, m_i)$ (Eq.(A5)) with $w = 1$ and $\delta_0 = 2$ in panel (a) and Eq.(A4) in panel (b) for $\delta t_0 = 120$ sec and for different values of σ (see legend). The legend also reports the percentage of earthquakes removed from the original complete catalog. The magenta dashed line is the theoretical GR law with $b_{true} = 1$.

or with $m_{i+l} \geq m_i + \delta M_{\text{th}}$, in the b-positive or b-more-positive estimator, respectively. For the b-more-incomplete estimator, N_n corresponds to the number of earthquake pairs with $m_{i+l} \geq m_i$ in the n-th synthetic filtered catalog.

We assess the efficiency of the different estimators by plotting each average value as a function of the associated $\langle N \rangle$, recalling that the more efficient estimator is the one that, at a fixed $\langle N \rangle$, provides an estimate of the b-value closer to b_{true}.

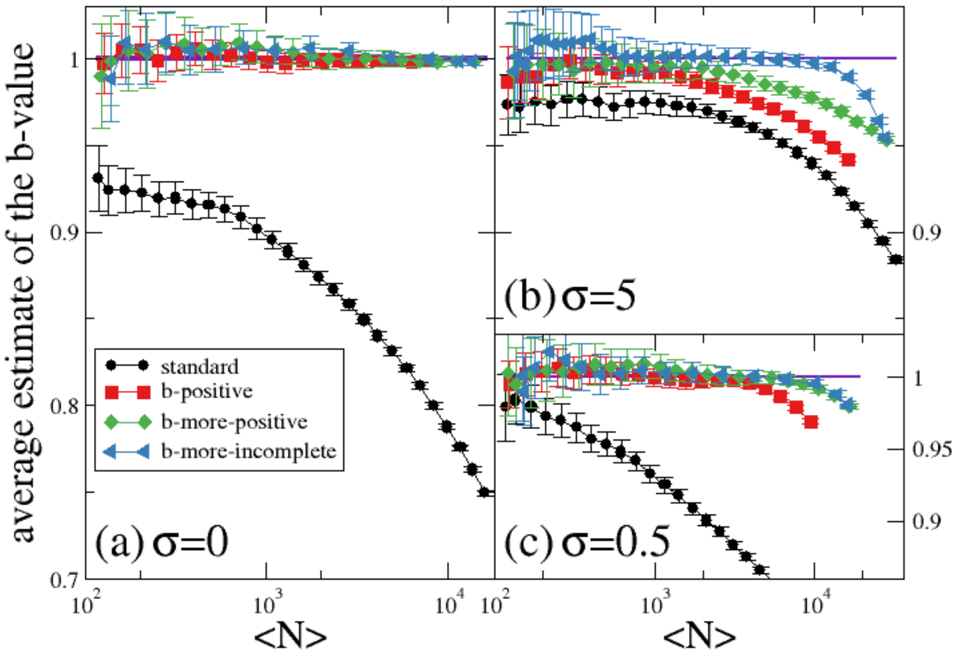

Figure 4. (Color online) The quantities $\langle b(M_{th}) \rangle$ (black circles), $\langle b_+(\delta M_{th}) \rangle$ (red squares), $\langle b_{+l}(\delta M_{th}) \rangle$ (green diamonds), and $\langle b_+^f(\tau) \rangle$ (blue triangles) are plotted as a function of the average number of earthquakes $\langle N \rangle$ used for their evaluation in the synthetic catalog where STAI is implemented according to the detection magnitude $M_t(t - t_i, m_i)$ defined in Eq.(A5) with $w = 1$ and $\delta_0 = 2$. Error bars representing the relative standard deviation are indicated for each quantity. The solid indigo line represents the exact b-value $b_{true} = 1$. Different panels correspond to different choices of σ: $\sigma = 0$ (a), $\sigma = 5$ (b), and $\sigma = 0.5$ (c). Note that panels (a) and (b) share the same vertical axis scale, while panel (c) is limited to b-value estimates greater than 0.86.

5.1 Single Omori Sequence

We consider the first 14 days of a seismic sequence triggered by a magnitude 8 mainshock. We assume that SNDI is not relevant, and incompleteness is solely caused by STAI. Specifically, we assume that STAI influence the detection function $\Phi(m - M_c)$, with M_c as defined in Eq.(A3). We implement two different choices for $M_t(t - t_i, m_i)$: one using Eq.(A4) with $\delta t_0 = 120$ sec, and the other using Eq.(A5) with $w = 1$ and $\delta_0 = 2$.

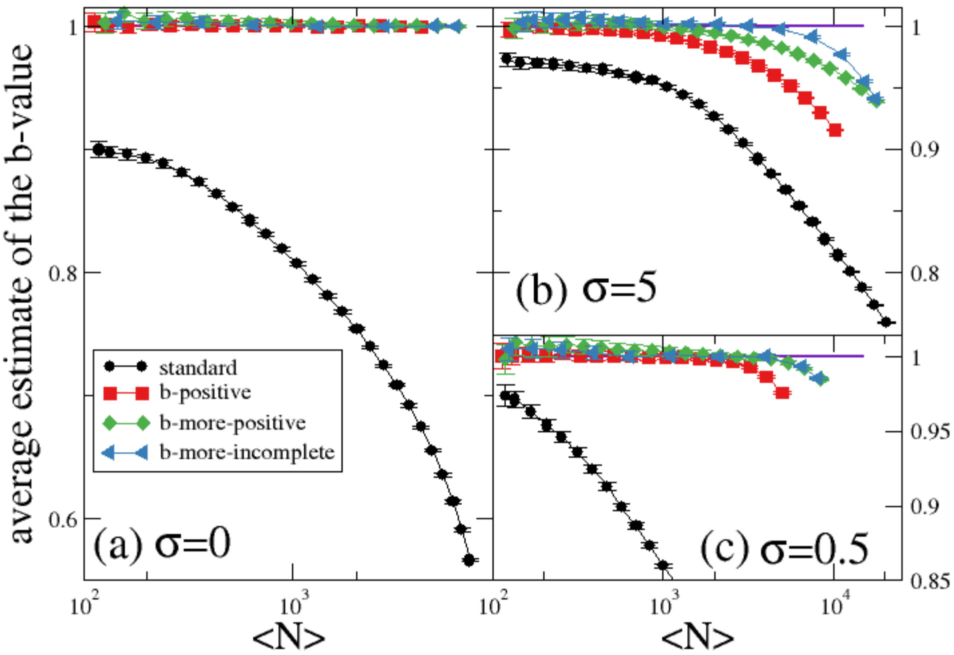

Figure 5. (Color online) The same of Fig.4 for the synthetic catalog where STAI is implemented according to the detection magnitude $M_t(t - t_i, m_i)$ defined in Eq.(A4) with $\delta t = 120$ sec.

For the two different choices of $M_t(t-t_i, m_i)$, the effect of the detection function Φ on the magnitude distribution for various values of σ is depicted in Fig.3a and Fig.3b, respectively. Furthermore we plot $\langle b(M_{th})\rangle$, $\langle b_+(\delta M_{th})\rangle$, $\langle b_{+l}(\delta M_{th})\rangle$, and $\langle b_+^f(\tau)\rangle$ for different values of σ as functions of $\langle N\rangle$, in Fig.4 and Fig.5 for the two different choices of $M_t(t-t_i, m_i)$, respectively. It's important to note that $\langle N\rangle$ decreases with increasing values of M_{th}, δM_{th}, and τ. The highest value of $\langle N\rangle$ for each curve corresponds to $M_{th} = 0$, $\delta M_{th} = 0$, and $\tau = 0$, respectively.

In Fig.4a, we consider the case where $\sigma = 0$. This figure reveals that due to the significant incompleteness (with over 94% of earthquakes removed), the traditional method fails to provide an accurate estimate of the b-value. This is evident from $\langle b(M_{th})\rangle$ consistently being smaller than b_{true} even for $M_{th} > 3.8$. In contrast,$\langle b_+(\delta M_{th})\rangle \simeq \langle b_{+l}(\delta M_{th})\rangle \simeq b_{true}$ even for $\delta M_{th} = 0$. However, it's important to note that the largest number of earthquake pairs $\langle N\rangle$ used in the evaluation of $\langle b_+(\delta M_{th})\rangle$, corresponding to $M_{th} = 0$, is only half of the average number of events in the synthetic catalog. On the other hand, the largest number of earthquake pairs $\langle N\rangle$ used in the evaluation of $\langle b_{+l}(\delta M_{th})\rangle$, still corresponding to $M_{th} = 0$, represents more than 90% of the events in the synthetic catalog. Therefore, the b-more-positive estimator proves to be more efficient than the b-positive estimator due to its smaller uncertainty, δb_{+l}. Results for $\langle b_+^f(\delta\tau)\rangle$ closely resemble those for $\langle b_{+l}(\delta M_{th})\rangle$, indicating similar efficiency for both the b-more-positive and b-more-incomplete estimators.

In Fig.4b, we explore the case where $\sigma = 5$, which is an unrealistic situation but helps investigate the role of σ in the b-value estimate. We observe that in this case, the traditional estimator provides a more accurate estimate of the b-value compared to the $\sigma = 0$ case (panel a). This improvement is attributed to the fact that increasing σ leads to a more complete catalog (Fig.1) even if significant deviations from the true b-value are still present also for large values of M_{th}. Concerning the b-positive estimator, the counter intuitive behavior is that even though the catalog for $\sigma = 5$ is more complete than the $\sigma = 0$ one, it provides a less accurate estimate of the b-value. A reasonable estimate is achieved only for $\delta M_{th} \gtrsim 1.5$, corresponding to $\langle N\rangle < 400$. Similar considerations also apply to the b-more-positive estimator that, however, for each value of $\langle N\rangle$, provides an estimate of the b-value that is consistently closer to b_{true} compared to the one provided by the b-positive estimator. Finally, Fig.4b shows that an even more efficient estimate of the b-value is achieved with the b-more-incomplete estimator, which provides a value close to b_{true} already for $\langle N \rangle > 8000$. In Fig.4c, we present the case for the more realistic situation where $\sigma = 0.5$. We emphasize that for this value of σ, even though the catalog remains significantly incomplete (with about 90% of earthquakes removed), the estimate of the b-value provided by the b-positive estimator differs from the true b-value, b_{true}, by less than 5%, even for $\delta M_{th} = 0$. Accuracy improves with increasing δM_{th}, with a highly accurate estimate obtained for $\langle N \rangle \simeq 4000$, corresponding to $\delta M_{th} = 0.5$. An even more accurate b-value estimate is achieved by the b-more-positive and b-more-incomplete estimators, which consistently provide estimates of the b-value that are closer to b_{true} for each $\langle N \rangle$ compared to the value provided by the b-positive estimator. The traditional estimator, on the other hand, consistently underestimates the b-value for all $\langle N \rangle$ values.

In Fig.5, we repeat the same analysis as in Fig.4 but consider a detection function that uses M_t provided by Eq.(A4) with $\delta t_0 = 120$. Fig.5 confirms all the conclusions drawn from the analysis of Fig.4, indicating that the b-positive estimator is generally a very efficient strategy for measuring the b-value in the presence of STAI. Additionally, the b-more-positive and b-more-incomplete estimators are even more efficient procedures, particularly in scenarios with higher σ values.

5.2 Background activity

We generate a numerical catalog where earthquakes are Poisson-distributed in time, with the occurrence probability in the position ($\vec{x}$) given by the background rate in Southern California obtained in Petrillo and Lippiello (2020). The catalog covers a period of 20 years, and since, by construction, the catalog does not present aftershock sequences, only a few events will be removed due to STAI. The only source of incompleteness is therefore represented by SNDI, which is implemented by assigning a completeness threshold M_R that varies in different positions. More precisely, we divide the region into grids of size $0.2° \times 0.2°$ and assign to each grid an incompleteness level M_R, randomly extracted from the range $[1 : 4]$. A smoothing procedure is then applied over a smoothing distance of $0.2°$. We then assume the detection function $\Phi(m - M_r(\vec{x}))$ with $\Phi(x)$ defined in Eq.(2) and consider different values of σ. The number of removed earthquakes increases as σ decreases, as evident from the magnitude distribution (Fig. 6).

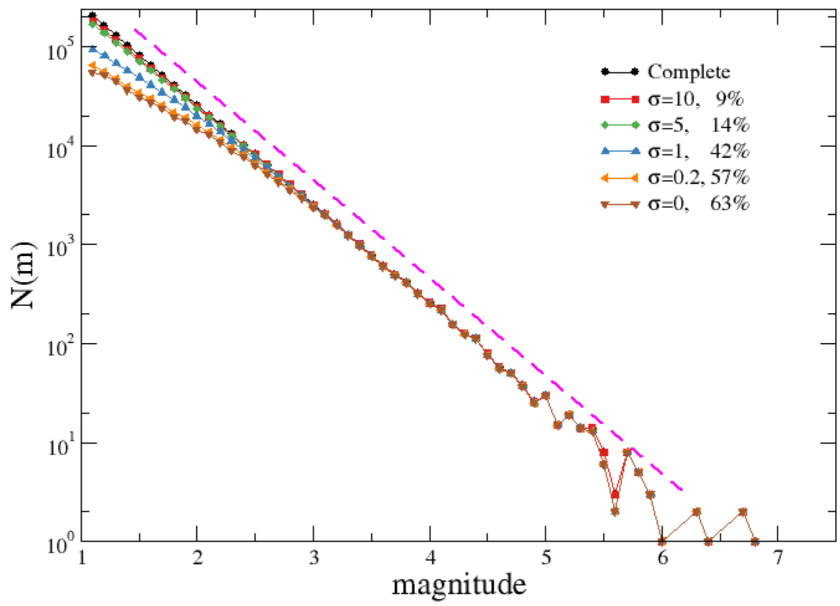

Figure 6. (Color online) The number of earthquakes $N(m)$ with magnitude in $[m, m + 1)$ in the numerical catalog of background earthquakes presenting SNDI with different values of σ (see legend). The legend reports the percentage of earthquakes removed from the original complete catalog. The magenta dashed line is the theoretical GR law with $b_{true} = 1$.

We remark that $b_+^f(\tau)$ is practically indistinguishable from $b_{+l}(\delta M_{th} = 0)$ for reasonable values of $\tau < 1000$ sec. Accordingly, the quantity $b_+^f(\tau)$ is not of interest in this situation and is not considered. We, therefore, focus on the comparison between the traditional, the b-positive, and the b-more-positive estimators. For the latter estimator, we consider the effect of the constraint on the epicentral distance between the earthquakes i and j, $d_{ij} < d_R$, exploring different values of d_R.

In Fig. 7, we consider the cases $\sigma = 0$ and $\sigma = 1$. We observe that for both values of σ, the b-positive estimator provides a less accurate estimate of the b-value compared to the traditional estimator. This result shows that the b-positive estimator is not appropriate for managing SNDI if the further constraint $d_{ij} < d_R$ is not imposed. The b-more-positive estimator, conversely, even without imposing the spatial constraint, i.e. $d_R = \infty$, is more efficient than the traditional estimator. This is due to the use of a large number of earthquake pairs, compared to the b-positive estimator, as discussed in Sec.3.2. Nevertheless, without a spatial constraint, the estimate of the b-value remains inaccurate, even for $\sigma = 0$. At the same time, Fig. 7 shows that, implementing a more stringent constraint, $\langle b_{+l}(\delta M_{th})\rangle$ better approximates b_{true} as the value of d_R decreases. In particular, when $\sigma_R = 0$, $\langle b_+(\delta M_{th})\rangle$ with $d_R = 0.01°$ provides an accurate estimate of b_{true} even for $\delta M_{th} = 0$.

6 Experimental data

In this section, we focus on the 2019 Ridgecrest Sequence, which has been extensively investigated by van der Elst (2021) using the b-positive method. Therefore, we can make a better comparison with existing results. We present results for the complete aftershock zone identified by van der Elst (2021), corresponding to a lat/lon box with corners $[35.2, -118.2], [36.4, -117.0]$. We restrict our study to the temporal window of 10 days following the $M6.4$ foreshock (Fig. 8a), including all earthquakes with $m_i \geq m_L = 0$ present in the USGS Comprehensive Catalog. The short-term incompleteness of the data set is clearly visible in the temporal window of a few days following the $M6.4$ foreshock and, even more clearly, after the $M7.1$ mainshock, when only a few small earthquakes are reported in the catalog.

We first consider the entire 10-day time window and plot $b(M_{th})$, $b_+(\delta M_{th})$, $b_{+l}(\delta M_{th})$, and $b_+^f(\tau)$ as a function of the number of earthquakes N used in their evaluation. Re-

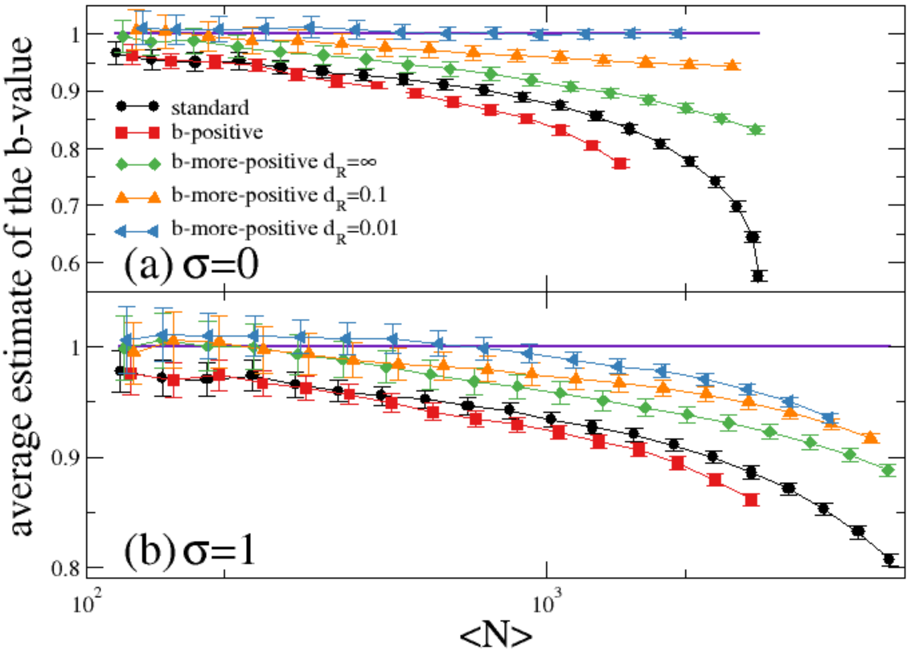

Figure 7. (Color online) The quantities $\langle b(M_{th})\rangle$ (black circles), $\langle b_+(\delta M_{th})\rangle$ (red squares) and $\langle b_{+l}(\delta M_{th})\rangle$ are plotted versus the number of earthquakes $\langle N\rangle$ used for their evaluation. In the case $\langle b_{+l}(\delta M_{th})\rangle$ we use different colors and symbols to indicate different values of d_R (see legend). Error bars indicate the standard deviation associated to each quantity. The continuous indigo line represents the exact b-value b_{true}. Different panels correspond to different choices of σ: $\sigma = 0$ (a), $\sigma = 1$ (b).

sults are plotted in Fig.9, where error bars indicate the standard error obtained via bootstrapping. For the considered data set, the constraint $d_{ij} < d_R$ on spatial distance does not produce any advantage since aftershocks, by selection, occur in a region with similar seismic network coverage, and also because incompleteness is mostly affected by STAI in the first part of the sequence.

Results plotted in Fig.9 show that, as expected, $b(M_{th})$ strongly depends on N, i.e., it strongly depends on M_{th}, and only for $M_{th} \geq 3.7$ does it appear to converge to a reasonably stable value $b \simeq 1$. Nevertheless, for $M_{th} \geq 3.7$, $N < 250$, and this implies that fluctuations in the estimate of b are of the order of 10%, which does not allow for an accurate estimate of the b-value. It is worth noticing that the condition $N < 250$ is obtained by focusing on the whole time window of 10 days, and therefore, it is obvious that the evaluation of $b(M_{th})$ on shorter time windows is even more dominated by fluctuations. This implies that the traditional estimator based on $b(M_{th})$ is not suitable for describing the temporal evolution of the b-value in the temporal window after large earthquakes. Since the mechanism responsible for the presence of the time-dependent completeness magnitude is expected to be quite universal (Sec.2), it is reasonable to assume that this consideration, obtained for the Ridgecrest sequence, generally applies to other sequences.

At the same time, Fig. 9 shows that the dependence of $b_+(\delta M_{th})$ on N, or equivalently on δM_{th}, is much smoother, with $b_+(\delta M_{th})$ ranging from the initial value $b_+(\delta M_{th}) = 0.88 \pm 0.01$ for $\delta M_{th} = 0$ to a stable value $b_+(\delta M_{th}) = 0.96 \pm 0.02$ for $\delta M_{th} \gtrsim 0.5$. Interestingly, Fig. 9 confirms that the b-more-positive and the b-more-incomplete estimators are able to provide an accurate estimate of the b-value preserving a large value of N. Indeed, the b-more-positive estimator consistently provides a stable estimate of the b-value, remaining approximately constant at $b_{+l}(\delta M_{th}) = 0.96 \pm 0.01$ even when using a substantial dataset with $N > 10^4$. This allows us to consider sample sizes approximately twice as large as those required for the b-positive estimator and a remarkable 30 times larger than what the traditional estimator can handle. Similarly, the b-more-incomplete estimator exhibits the same favorable characteristics, making it well-suited for tracking the temporal evolution of the b-value.

Accordingly, we use results from Fig.9 to determine suitable values for δM_{th} and τ to obtain a reliable estimate of b using either $b_+(\delta M_{th})$, $b_{+l}(\delta M_{th})$, or $b_+^f(\tau)$. Our re-

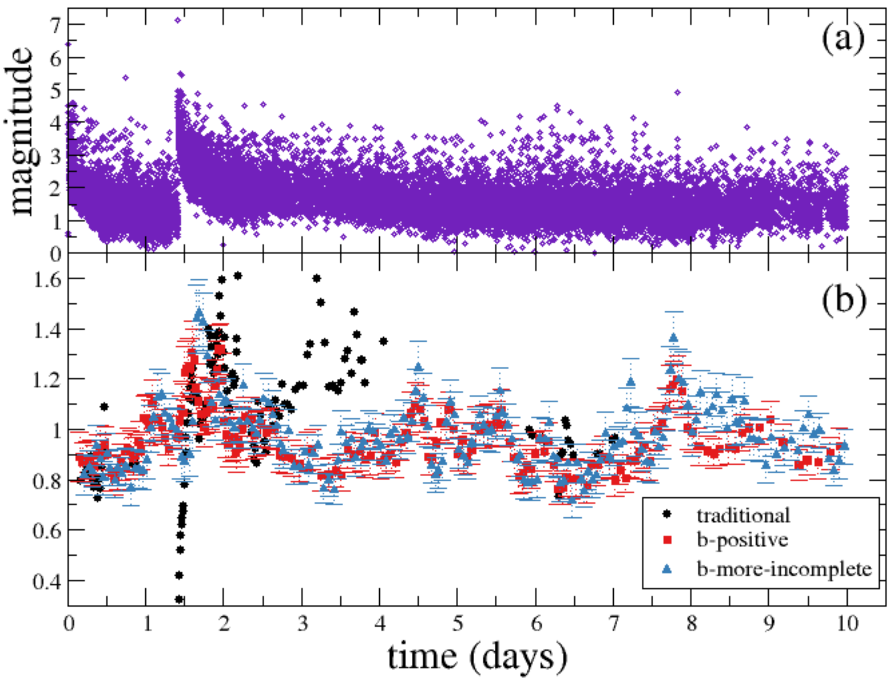

Figure 8. (Color online) (a) Magnitudes versus time for the Ridgecrest 2019 sequence. (b) The quantities $b(M_{th} = 3)$ (black circles), $b_+(\delta M_{th} = 0.2)$ (red squares) and $b_+^f(\tau = 120)$ (blue triangles) are plotted versus time for the Ridgecrest 2019 sequence. Error bars represent the standard deviation for the latter two quantities, obtained through bootstrapping.

sults indicate that $\delta M_{th} = 0.3$ is appropriate for both the b-positive and the b-more-positive estimators, although we present very similar results obtained with $\delta M_{th} = 0.2$ to align with the choice made by van der Elst (2021) in his study. Additionally, we employ $\tau = 120$ seconds for $b_+^f(\tau)$. It's worth noting that we find that our results are robust and only minimally influenced by different choices of δM_{th} and τ, as expected based on the weak dependence on N observed in Fig.9.

To explore the temporal evolution of the b-value, we followed the method used by van der Elst (2021), dividing the 10-day interval into overlapping sub-intervals containing 400 events each, and calculating $b_+(\delta M_{th} = 0.2)$, $b_{+l}(\delta M_{th} = 0.2)$, and $b_+^f(\tau = 120)$ for each sub-interval. We found that $b_+(\delta M_{th} = 0.2)$ and $b_{+l}(\delta M_{th} = 0)$ are very similar and we therefore plot only $b_+(\delta M_{th} = 0.2)$ together with $b_+^f(\tau = 120)$ in Fig.8b as a function of the final time of each sub-interval. Note that the effective number of earthquakes N used in the evaluation of the three quantities in each sub-interval is always smaller than 400. In Fig.8b, for comparison, we also plotted the temporal evolution of $b(M_{th})$ with $M_{th} = 3$, chosen to reduce the effect of incompleteness while keeping a sufficient number $N > 10$ of earthquakes for its evaluation in each sub-interval. Data for $b(M_{th})$ are plotted without error-bars to preserve the clarity of the figure.

The behavior of $b_+(\delta M_{th} = 0.2)$ is consistent (Fig.8b) with the results obtained by van der Elst (2021). Specifically, we observe a small value of b_+ after the M6.4 foreshock, a recovery of the pre-foreshock value immediately before the M7.1 mainshock, and a value that remains high immediately after the mainshock before decaying to an asymptotic value that fluctuates around $b_+ \simeq 1$. This trend is also confirmed by $b_+^f(\tau = 120)$ (Fig. 8b), although it exhibits some differences with $b_+(\delta M_{th} = 0.2)$. In general, these differences always remain within statistical uncertainty except for the temporal window located about 2 hours after the $M7.1$ mainshock, where $b_+^f(\tau = 120)$ presents an anomalous large value $b_+^f(\tau = 120) = 1.45$ significantly larger than the value presented by $b_+(\delta M_{th} = 0.2)$. The overall behavior of $b_+^f(\tau = 120)$ confirms the observation made by van der Elst (2021) of a reduction in the b-value between the foreshock and mainshock, compared to the previous temporal window and, in particular, compared to the temporal window after the mainshock. This feature has been proposed by Gulia and Wiemer (2019); Gulia et al. (2020) as a precursory pattern for large earthquake forecasting. However, in agreement with the b-positive estimate by van der Elst (2021), our results from b_{+l} and b_+^f show that this pattern is less pronounced compared to the one obtained from

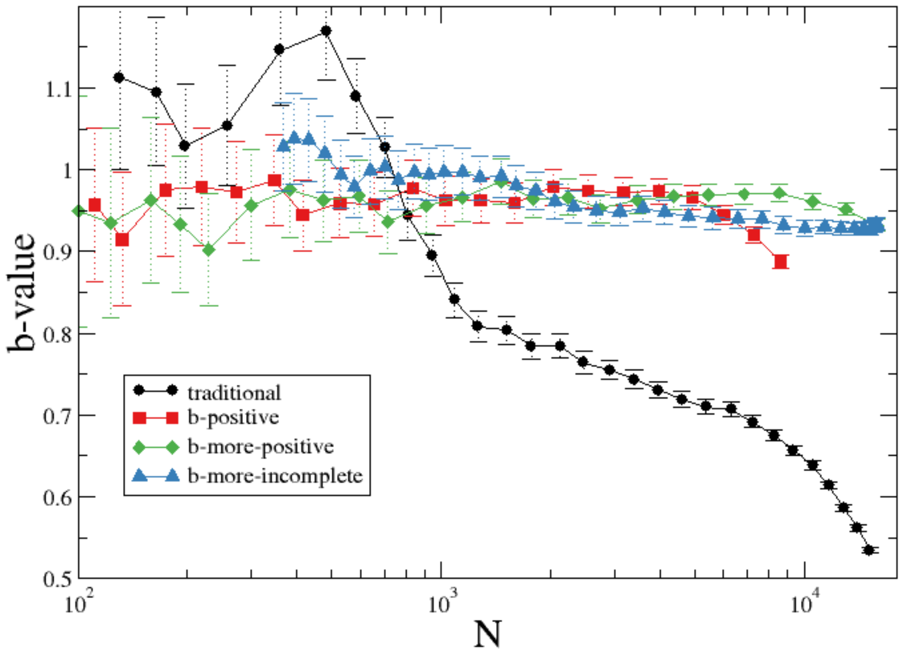

Figure 9. (Color online) The quantities $b(M_{th})$ (black circles), $b_+(\delta M_{th})$ (red squares), $b_{+l}(\delta M_{th})$ (green diamonds) and $b_+^f(\tau)$ (blue triangles) are plotted versus the number of earthquakes N used for their evaluation, for the whole period of 10 days during the Ridgecrest 2019 sequence. Error bars represent the standard deviation obtained through bootstrapping

$b(M_{th})$, making its identification more challenging. Similar conclusions can be drawn for other fore-mainshock sequences, including the 2016 Amatrice-Norcia, Italy, sequence, the 2016 Kumamoto, Japan, sequence, and the 2011 Tohoku-oki, Japan, sequence, which have also been analyzed by van der Elst (2021). Similarly, in these additional sequences, the outcomes derived from the b-more-positive and b-more-incomplete estimators (not shown) align closely, within statistical uncertanty, with the results obtained using the b-positive estimator in van der Elst (2021).

7 Discussions

We have obtained an analytical expression for the probability distribution of the magnitude difference $\delta m = m_j - m_i$, where $j = i + l$, with $l \geq 1$, and restricting to positive δm, under the assumption that for all intermediate magnitudes $m_j < m_i$ with $j \in [i+1, i+l-1]$. We have found that for a complete data set obeying the GR law with coefficient b, $p_l(\delta m) = K_l 10^{-b\delta m}$. The coefficient, K_l, exhibits a dependence on l, taking on the value of $K = 1/2$ when $l = 1$, as in the b-positive estimator proposed by van der Elst (2021). This value of $K_l = 1/2$ reflects the average occurrence where half of the earthquakes m_i are succeeded by larger ones. We have demonstrated that as l increases K_l approaches 1, in the novel estimator defined as the b-more-positive. Consequently, an accurate measurement of the b-value can be derived from the probability distribution $p_l(\delta m)$, with the procedure growing in efficiency as l increases, allowing for the inclusion of a larger number of earthquakes in the measurement.

The intriguing point is that even for incomplete datasets, the probability distribution $p_l(\delta m)$ can exhibit the same exponential decay pattern, namely $p_l(\delta m) = K 10^{-b\delta m}$, with incompleteness only affecting the constant K which remains smaller than K_l. This phenomenon occurs when the detection probability for observing the subsequent earthquake m_{i+l}, given that earthquake m_i has been detected and reported in the catalog, approaches unity. Achieving this condition can be straightforward by taking advantage of the fact that the completeness magnitude decreases over time. Indeed, it can be achieved by simply imposing the constraint that $m_{i+l} > m_i + \delta M_{th}$. Since values of δM_c typically on the order of 0.2 are usually sufficient, this strategy enables us to utilize a significant portion of the initial dataset in the measurement of the b-value. In contrast, in the traditional estimator, we were forced to exclude all earthquakes above a threshold M_{th}, which generally led to a substantial reduction in the dataset. In addition, we have introduced the b-more-incomplete estimator. This estimator is derived by assessing the distribution of magnitude differences within a catalog that has undergone pre-filtering to exclude earthquakes with a magnitude below a specified artificial detection threshold $M_A \gtrsim M_c$. It has been demonstrated that this estimator exhibits greater efficiency in the presence STAI. This enhanced performance can be attributed to the exclusion of all pairs with $\delta m < \delta M_{th}$ in the 'b-more-incomplete' estimator, while the standard 'b-more-incomplete' estimator employs a more targeted exclusion process.

In general, we do not expect significant differences in the measurement of the b-value provided by the different estimators based on the distribution of positive magnitude differences. The main difference lies in the reduction of statistical fluctuations, which are less pronounced in the b-more-positive and b-more-incomplete estimators. This reduction can be very important in detecting potential variations in the b-value during real-time earthquake sequences.

We finally observed that the novel b estimators can also be useful in addressing spatial incompleteness, which is related to the spatial density of seismic stations, by imposing that two earthquakes m_{i+l} and m_i occur in regions with the same completeness magnitude.

8 Conclusions

The b-positive estimator, as proposed by van der Elst (2021), provides a measure of the b-value based solely on the positive differences between successive earthquake magnitudes. We have identified the mathematical motivation that makes this new estimator significantly more efficient than the traditional approach, which measures the b-value using a dataset that includes only earthquakes larger than a fixed threshold M_{th}. The key insight is that incompleteness only affects the magnitude difference distribution through the detection probability of observing a subsequent earthquake, conditioned on the prior earthquake being detected and reported in the catalog (see Eq.(13)). Since the completeness level generally decreases over time, the detection probability tends to approach one in most situations, and the magnitude difference distribution remains largely unaffected by incompleteness. We've clarified that to satisfy this condition, it's necessary for both earthquakes to occur within regions with similar seismic coverage. Consequently, we've demonstrated that the b-positive estimator is effective only when the epicentral distance between earthquakes i and j is smaller than a reference threshold, denoted as d_R.

Furthermore, we've introduced a more efficient variant called the b-more-positive estimator. Unlike the b-positive estimator, which considers only positive magnitude differences between successive earthquakes and thus analyzes only half of the earthquakes in the catalog, the b-more-positive estimator evaluates the magnitude difference between m_i and the subsequent earthquake, denoted as m_{i+l}, under the condition that $m_{i+l} > m_i$ and all intermediate earthquakes $m_j < m_i$ with $j \in [i+1, i+l-1]$. The distribution of $m_{i+l}-m_i$ retains all the characteristics of the distribution $m_{i+1}-m_i$, allowing us to use the entire earthquake dataset, rendering the b-more-positive estimator more efficient.

We also emphasize a limitation of the b-positive estimator, stemming from the fact that if some earthquakes with $m_i < M_c$ are reported in the catalog, the detection probability to observe a subsequent earthquake $m_j > m_i$ is no longer equal to one. This leads to the counter intuitive behavior that the more earthquakes below M_c are reported in the catalog, i.e., the more complete the dataset, the less accurate the b-positive estimator becomes. This issue can be resolved, as proposed by van der Elst (2021), by imposing $m_j - m_i > \delta M_{th}$ to ensure that $m_j > M_c$ always holds, guaranteeing a detection probability of one. However, we demonstrate a more efficient approach by introducing an artificial, time-dependent magnitude threshold, denoted as M_A, and filtering the catalog by removing all earthquakes with $m_i < M_A$. By appropriately tuning M_A, this approach, referred to as the b-more-incomplete estimator, results in a detection probability of one and provides a more efficient measurement of the *b*-value.

This comprehensive framework is supported by extensive numerical simulations, which validate the analytical prediction that the b-positive method becomes more efficient as the dataset's incompleteness increases.

We also applied the new methodologies to real main-aftershock sequences. Specifically, we compared the *b*-value obtained from the b-positive estimator, as previously done by van der Elst (2021) during the 2019 Ridgecrest sequence, with the new measurements provided by the b-more-incomplete and b-more-positive estimators. Our findings revealed very similar results across these different measurement methods, with reduced statistical fluctuations observed in the novel estimators due to their enhanced efficiency. This strengthened our ability to support the conclusions drawn by van der Elst (2021), particularly regarding the significant decrease in the *b*-value after the M6.4 aftershock, in comparison to its prior value and the value following the M7.1 mainshock. We noted a similar consensus among the various estimators when assessing the b-value in the other three fore-main-aftershock sequences investigated by van der Elst (2021). In summary, the application of the novel b-value estimators to the instrumental catalog allowed us to mitigate statistical fluctuations. However, it did not introduce new insights beyond the conclusions previously presented by van der Elst (2021) concerning the feasibility of incorporating *b*-value variations into a real-time earthquake alarm system.

Finally, we emphasize that measuring the *b*-value using the b-more-positive estimator can be particularly advantageous for short-term post-seismic forecasting. It can be effectively combined with procedures based on the envelope of seismic waveforms (Lippiello et al., 2016; Lippiello, Cirillo, et al., 2019; Lippiello, Petrillo, Godano, et al., 2019), which facilitate the extraction of Omori-Utsu law parameters but do not provide access to the b-value.

9 Open Research

[Data] The seismic catalog for the Ridgecrest sequence is taken from the USGS Comprehensive Catalog (https://earthquake.usgs.gov/earthquakes/search/). [Software] Numerical codes for the b-more-positive and b-more-incomplete methods are available at https://zenodo.org/badge/latestdoi/611337136 (2023).

Appendix A SNDI and STAI

The Seismic Network Density Incompleteness (SNDI) at a specific spatial position $\vec{x}$ is contingent upon the number of seismic stations surrounding that location. As an illustration, in the context of Taiwan seismicity, Mignan et al. (2011) determined a completeness magnitude $M_R(\vec{x})$ that exhibits a correlation with the distance $d(\vec{x}) = |\vec{x} - \vec{x}_k|$ defined by the equation

$$M_R(\vec{x}) = 4.81 d(\vec{x})^{0.09} - 4.36. \tag{A1}$$

In this expression, $\vec{x}_k$ represents the coordinates of the nearest seismic station to the earthquake's epicenter, with k signifying the minimum number of stations needed for earthquake localization. Eq. (A1) applies when $k = 3$. A similar correlation between completeness magnitude and the number of seismic stations has also been established by Schorlemmer and Woessner (2008), who employed network-specific attenuation relations and station information. The value of $M_R(\vec{x})$ can vary over time due to factors such as day-night variations, seasonal changes, changes in duty personal, and so on. These variations can be accounted for by assuming that $M_R(\vec{x})$ exhibits fluctuations on the order of σ, which will manifest in the detection function $\Phi(m - M_R(\vec{x}))$ (see Eq.(2)).

Short-Term Aftershock Incompleteness (STAI) is a time-dependent property that changes rapidly in the aftermath of a large earthquake. Empirical observations (Kagan, 2004; Helmstetter et al., 2006) indicate that STAI can be described in terms of a completeness magnitude depending on time t since the mainshock $M_C = M_T(t)$ and exhibiting a logarithmic dependence on the temporal distance from the mainshock. The equation below describes (Kagan, 2004; Helmstetter et al., 2006) $M_T(t)$, where m_M is the magnitude of the mainshock, and $q \approx 1$ and $\Delta m \in [4, 4.5]$ (with time measured in days) are two fitting parameters

$$M_T(t) = m_M - q\log(t) - \Delta m, \tag{A2}$$

at a temporal distance $t > 0$ after the mainshock. Eq.(A2) originates from the obscuration of small aftershocks which are hindered by coda waves of previous larger ones. This obscuration effect, responsible for STAI, can be incorporated (Lippiello, Petrillo, Godano, et al., 2019) introducing, after each aftershock with magnitude m_i occurring at time the t_i, a detection magnitude $M_t(t-t_i, m_i)$ leading to a completeness magnitude at the time t

$$M_T\left(t|\mathcal{H}_i\right) = \max_{t_i<t} M_t(t-t_i, m_i) \tag{A3}$$

where the maximum must be evaluated over all the earthquakes occurred up to time t_i which are indicated in the compact notation $\mathcal{H}_i$. Different functional forms have been proposed for $M_t(t-t_i, m_i)$

$$M_t(t-t_i, m_i) = \begin{cases} m_i & \text{if } t-t_i < \delta t_0 \\ m_L & \text{if } t-t_i \geq \delta t_0 \end{cases} \tag{A4}$$

$$M_t(t-t_i, m_i) = m_i - w\log(t-t_i) - \delta_0, \tag{A5}$$

$$M_t(t-t_i, m_i) = \nu_0 + \nu_1 \exp\left(-\nu_2\left(3+\log(t-t_i)\right)^{\nu_3}\right). \tag{A6}$$

Here Eq.(A4) is inspired by the hypothesis of a constant blind time δt_0 proposed by Hainzl (2016b, 2016a, 2021), according to which an earthquake hides all subsequent smaller ones if they occur at a temporal distance smaller than δt_0. Eq.(A5) implements the functional form of $M_T(t)$ in Eq.(A2), whereas Eq.(A6) is the one proposed by Ogata and Katsura (2006). Eq.(A5) is also the one implemented by van der Elst (2021) in his study. In this manuscript, we consider the first two functional forms, which both reproduce statistical features of aftershocks in instrumental catalogs, even if Eq.(A5) better captures magnitude correlations between subsequent aftershocks (de Arcangelis et al., 2018).

Appendix B Analytical calculation for the distribution of magnitude difference.

B1 Probability distribution $p(\delta M)$ in complete data sets

The cumulative probability of observing a magnitude difference $m_j - m_i > \delta m$ between two generic earthquakes recorded in a catalog can be expressed as:

$$P(\delta m) = \int_{m_L}^{\infty} dm_i \int_{m_i+\delta m}^{\infty} dm_j \int_0^T dt_i \int_\Omega d\vec{x}_i \int_{t_i}^{T} dt_j \int_\Omega d\vec{x}_j \, p\left(m_j, t_j, \vec{x}_j|\mathcal{H}_j\right) \, p\left(m_i, t_i, \vec{x}_i|\mathcal{H}_i\right), \tag{B1}$$

where $\mathcal{H}_i$ and $\mathcal{H}_i$ are used to represent the seismic history before the occurrence of the i-th and the j-th event, respectively. The integrals in space extend over the entire region Ω covered by the catalog, and the integral in time for t_i extends over the entire temporal period $[0, T]$ covered by the catalog, with the constraint $t_j > t_i$ imposed for the integral in time for t_j.

In the subsequent analysis, we assume that magnitudes do not depend on occurrence time and space and follow the GR law given by Eq.(1) for magnitudes $m_i \geq m_L$. Correlations with previous seismicity are introduced through the detection issues discussed in Sec.2, leading to Eq.(4) which used in Eq.(B1) leads to

$$\begin{aligned} P(\delta m) \quad & = \beta^2 \int_{m_L}^{\infty} dm_i \int_{m_i+\delta m}^{\infty} dm_j \int_0^T dt_i \int_\Omega d\vec{x}_i \int_{t_i}^{T} dt_j \int_\Omega d\vec{x}_j \\ & e^{-\beta(m_j+m_i-2m_L)} \Lambda(t_j, \vec{x}_j) \Lambda(t_i, \vec{x}_i) \Phi\left(m_j - M_c\left(t_j, \vec{x}_j, \mathcal{H}_j|\, m_i\right)\right) \\ & \Phi\left(m_i - M_c\left(t_i, \vec{x}_i, \mathcal{H}_i\right)\right) \end{aligned} \tag{B2}$$

In the above equation we explicitly use the notation $\Phi\left(m_j - M_c|m_i\right)$ to specify that the detection functions must be evaluated in conditions such as the previous earthquake m_i has been identified and reported in the catalog.

In the ideal case where all earthquakes have been reported in the catalog, i.e., $\Phi(m_i - M_c) = 1$ and $\Phi(m_j - M_c|m_i) = 1$ for all earthquakes, the integrals in Eq. (B2) over t_i, t_j, $\vec{x}_i$, $\vec{x}_j$, and m_j can be easily performed, resulting in

$$P(\delta m) = \beta e^{-\beta\delta m} \int_{m_L}^{\infty} dm_i e^{-2\beta(m_i-m_L)} = \frac{1}{2} e^{-\beta\delta m}. \tag{B3}$$

The probability density $p(\delta m)$ of having $m_j = m_i + \delta m$ can be obtained by taking the derivative of $P(\delta m)$ with respect to δm and changing the sign, ultimately leading to Eq.(8).

B2 Probability distribution $p(\delta M)$ in incomplete data sets

In the hypothesis that condition Eq.(13) holds, i.e. $\Phi(m_j - M_c|m_i) = 1$, even if Eq.(5) is not satisfied, i.e. $\Phi(m_i - M_c) < 1$ it is easy to show that Eq.(B2) gives

$$P(\delta m) = e^{-\beta\delta m} K \tag{B4}$$

with K a constant given by

$$K = \int_{m_L}^{\infty} dm_i \int_0^T dt_i \int_\Omega d\vec{x}_i \int_{t_i}^T dt_j \int_\Omega d\vec{x}_j e^{-2\beta(m_i - m_L)} \Lambda(t_i, \vec{x}_i) \Phi\left(m_i - M_c\left(t_i, \vec{x}_i, \mathcal{H}_i\right)\right). \tag{B5}$$

After deriving Eq.(B5) we finally obtain Eq.(14).

B3 Probability distribution $p_l(\delta M)$

We first consider the cumulative probability $P'_n(\delta m)$ to observe a magnitude difference $m_{i+n+1} - m_i > \delta m$, $n \geq 0$, between an earthquakes i and a subsequent earthquake $j = i + n + 1$, under the assumption that all intermediates earthquakes $k \in [i+1, i+n]$ $(t_k \in (t_i, t_j))$ presents a magnitude m_k smaller than m_i. We obtain

$$\begin{aligned} P'_n(\delta m) \quad &= \prod_{k=0}^{n} \int_{m_L}^{\infty} dm_i \int_{m_L}^{m_i} dm_k \int_{m_i+\delta m}^{\infty} dm_j \int_0^T dt_i \int_\Omega d\vec{x}_i \int_{t_i}^{t_j} dt_k \int_\Omega d\vec{x}_k \int_{t_{i+n}}^T dt_j \int_\Omega d\vec{x}_j \\ &p\left(m_j, t_j, \vec{x}_j|\mathcal{H}_j\right) p\left(m_k, t_k, \vec{x}_k|\mathcal{H}_k\right) p\left(m_i, t_i, \vec{x}_i|\mathcal{H}_i\right), \end{aligned} \tag{B6}$$

where we still indicate with $\mathcal{H}_k$ all the seismic history occurred before the occurrence of the k-th event.

In the case of a complete data set, we can utilize the factorization given in Eq. (4), enabling us to carry out integration over space and time. Additionally, the integration over m_j and m_k can be readily performed, ultimately leading to

$$P'_n(\delta m) = \beta e^{-\beta\delta m} \int_{m_L}^{\infty} dm_i e^{-2\beta(m_i - m_L)} \left(1 - e^{-\beta(m_i - m_L)}\right)^n. \tag{B7}$$

We now turn to consider the cumulative probability distribution $P_l(\delta M)$ of the magnitude difference $m_{i+l} - m_i$ between the magnitude of the i-th earthquake and the first subsequent earthquake which presents a magnitude $m_{i+l} > m_i$. It's important to note the distinction between P'_n and P_l. In the evaluation of P'_n, we assumed that the first subsequent earthquake with $m_j > m_i$ has occurred at the exact catalog position $j = i+n+1$. Conversely, in the evaluation of P_l, we must assume that the first subsequent earthquake with $m_j > m_i$ can occur at any catalog position $j = i+n+1$, with n taking all possible values in the range $[0, l]$. Accordingly, P_l can be obtained simply from

P'_n, with $P_l(\delta m) = \sum_{n=0}^{l} P'_n(\delta m)$. Using the property of a geometric series with a common ratio of $\left(1 - e^{-\beta(m_i - mL)}\right)$

$$\sum_{n=0}^{l} \left(1 - e^{-\beta(m_i - m_L)}\right)^n = \frac{1 - \left(1 - e^{-\beta(m_i - m_L)}\right)^{l+1}}{e^{-\beta(m_i - m_L)}} \tag{B8}$$

we obtain

$$P_l(\delta m) = \beta e^{-\beta \delta m} \int_{m_L}^{\infty} dm_i e^{-\beta(m_i - m_L)} \left(1 - \left(1 - e^{-\beta(m_i - m_L)}\right)^{l+1}\right). \tag{B9}$$

Next, by using the binomial expression, we obtain $P_l(\delta m) = K_l e^{-\beta \delta m}$ with

$$K_l = 1 - \sum_{k=0}^{l+1} (-1)^k \binom{l+1}{k} \frac{1}{k+1} \tag{B10}$$

which leads to

$$K_l = \frac{l}{l+1}, \tag{B11}$$

and after derivation to Eq.(10).

Acknowledgments

E.L. acknowledges support from the MIUR PRIN 2017 project 201798CZLJ. G.P. would like to thanks MEXT Project for Seismology TowArd Research innovation with Data of Earthquake (STAR-E Project), Grant Number: JPJ010217.

References

Aki, K. (1965). Maximum likelihood estimate of b in the formula $\log n = a - bm$ and its confidence limits. *Bull. Earthq. Res. Inst., Univ. Tokyo*, *43*, 237-239.

Amitrano, D. (2003). Brittle-ductile transition and associated seismicity: Experimental and numerical studies and relationship with the b value. *Journal of Geophysical Research: Solid Earth*, *108*(B1), 2044. Retrieved from `http://dx.doi.org/10.1029/2001JB000680` doi: 10.1029/2001JB000680

Bottiglieri, M., Lippiello, E., Godano, C., & de Arcangelis, L. (2011). Comparison of branching models for seismicity and likelihood maximization through simulated annealing. *Journal of Geophysical Research: Solid Earth*, *116*(B2), n/a–n/a. Retrieved from `http://dx.doi.org/10.1029/2009JB007060` (B02303) doi: 10.1029/2009JB007060

de Arcangelis, L., Godano, C., Grasso, J. R., & Lippiello, E. (2016). Statistical physics approach to earthquake occurrence and forecasting. *Physics Reports*, *628*, 1 - 91. Retrieved from `//www.sciencedirect.com/science/`

article/pii/S0370157316300011 doi: http://dx.doi.org/10.1016/j.physrep.2016.03.002

de Arcangelis, L., Godano, C., & Lippiello, E. (2018). The overlap of aftershock coda-waves and short-term post seismic forecasting. *Journal of Geophysical Research: Solid Earth*, *123*(7), 5661-5674. Retrieved from https://agupubs.onlinelibrary.wiley.com/doi/abs/10.1029/2018JB015518 doi: 10.1029/2018JB015518

Godano, C., Lippiello, E., & de Arcangelis, L. (2014). Variability of the b value in the Gutenberg–Richter distribution. *Geophysical Journal International*, *199*(3), 1765-1771. Retrieved from http://gji.oxfordjournals.org/content/199/3/1765.abstract doi: 10.1093/gji/ggu359

Godano, C., Petrillo, G., & Lippiello, E. (2023). Evaluating the incompleteness magnitude using an unbiased estimate of the b value. *arXiv*, *2307.03457*. Retrieved from https://arxiv.org/abs/2307.03457

Gulia, L., & Wiemer, S. (2010). The influence of tectonic regimes on the earthquake size distribution: A case study for italy. *Geophysical Research Letters*, *37*(10). Retrieved from https://agupubs.onlinelibrary.wiley.com/doi/abs/10.1029/2010GL043066 doi: 10.1029/2010GL043066

Gulia, L., & Wiemer, S. (2019). Real-time discrimination of earthquake foreshocks and aftershocks. *Nature*, *574*, 193-199. doi: 10.1038/s41586-019-1606-4

Gulia, L., Wiemer, S., & Vannucci, G. (2020). Pseudoprospective evaluation of the foreshock traffic-light system in ridgecrest and implications for aftershock hazard assessment. *Seismological Research Letters*, *91*, 2828—2842. doi: 10.1785/0220190307

Gutenberg, B., & Richter, C. (1944). Frequency of earthquakes in california,. *Bulletin of the Seismological Society of America*, *34*, 185–188.

Hainzl, S. (2016a). Apparent triggering function of aftershocks resulting from rate–dependent incompleteness of earthquake catalogs. *Journal of Geophysical Research: Solid Earth*, *121*(9), 6499–6509. Retrieved from http://dx.doi.org/10.1002/2016JB013319 (2016JB013319) doi: 10.1002/2016JB013319

Hainzl, S. (2016b). Rate-dependent incompleteness of earthquake catalogs. *Seismological Research Letters*, *87*(2A), 337-344.

Hainzl, S. (2021). ETAS-approach accounting for short-term incompleteness of earthquake catalogs. *Bulletin of the Seismological Society of America*, *112*, 494–507.

Helmstetter, A., Kagan, Y. Y., & Jackson, D. D. (2006). Comparison of short-term and time-independent earthquake forecast models for southern california. *Bulletin of the Seismological Society of America*, *96*(1), 90-106. Retrieved from http://www.bssaonline.org/content/96/1/90.abstract doi: 10.1785/0120050067

Kagan, Y. Y. (2004). Short-term properties of earthquake catalogs and models of earthquake source. *Bulletin of the Seismological Society of America*, *94*(4), 1207-1228.

Lippiello, E., Bottiglieri, M., Godano, C., & de Arcangelis, L. (2007). Dynamical scaling and generalized omori law. *Geophysical Research Letters*, *34*(23), L23301. Retrieved from http://dx.doi.org/10.1029/2007GL030963 doi: 10.1029/2007GL030963

Lippiello, E., Cirillo, A., Godano, C., Papadimitriou, E., & Karakostas, V. (2019, Aug). Post seismic catalog incompleteness and aftershock forecasting. *Geosciences*, *9*(8), 355. Retrieved from http://dx.doi.org/10.3390/geosciences9080355 doi: 10.3390/geosciences9080355

Lippiello, E., Cirillo, A., Godano, G., Papadimitriou, E., & Karakostas, V. (2016). Real-time forecast of aftershocks from a single seismic station signal. *Geophysical Research Letters*, *43*(12), 6252–6258. Retrieved from http://dx.doi.org/10.1002/2016GL069748 (2016GL069748) doi: 10.1002/2016GL069748

Lippiello, E., Godano, C., & de Arcangelis, L. (2012). The earthquake magnitude is influenced by previous seismicity. *Geophysical Research Letters*, *39*(5), L05309. Retrieved from http://dx.doi.org/10.1029/2012GL051083 doi: 10.1029/2012GL051083

Lippiello, E., Petrillo, C., Godano, C., Tramelli, A., Papadimitriou, E., & Karakostas, V. (2019). Forecasting of the first hour aftershocks by means of the perceived magnitude. *Nature Communications*, *10*, 2953. Retrieved from https://doi.org/10.1038/s41467-019-10763-3 doi: 10.1038/s41467-019-10763-3

Lippiello, E., Petrillo, G., Landes, F., & Rosso, A. (2019, 04). Fault Heterogeneity and the Connection between Aftershocks and Afterslip. *Bulletin of the Seis-*

mological Society of America, *109*(3), 1156-1163. Retrieved from https://doi.org/10.1785/0120180244 doi: 10.1785/0120180244

Lippiello, E., Petrillo, G. (2023, 09 14). caccioppoli/b-more-positive: b-more-positive:. Retrieved from Zenodo.https://zenodo.org/badge/latestdoi/611337136

Marzocchi, W., Spassiani, I., Stallone, A., & Taroni, M. (2019, 11). How to be fooled searching for significant variations of the b-value. *Geophysical Journal International*, *220*(3), 1845-1856. Retrieved from https://doi.org/10.1093/gji/ggz541 doi: 10.1093/gji/ggz541

Mignan, A., Werner, M. J., Wiemer, S., Chen, C.-C., & Wu, Y.-M. (2011). Bayesian estimation of the spatially varying completeness magnitude of earthquake catalogs. *Bulletin of the Seismological Society of America*, *101*(3), 1371-1385. Retrieved from http://www.bssaonline.org/content/101/3/1371.abstract doi: 10.1785/0120100223

Mignan, A., & Woessner, J. (2012). Estimating the magnitude of completeness in earthquake catalogs. *Community Online Resource for Statistical Seismicity Analysis*. Retrieved from http://www.corssa.org/export/sites/corssa/.galleries/articles-pdf/Mignan-Woessner-2012-CORSSA-Magnitude-of-completeness.pdf doi: 10.5078/corssa-00180805

Nanjo, K. Z. (2020). Were changes in stress state responsible for the 2019 ridgecrest, california, earthquakes? *Nature Communications*, *11*, 3082. doi: 10.1038/s41467-020-16867-5

Nanjo, K. Z., Hirata, N., Obara, K., & Kasahara, K. (2012). Decade-scale decrease in b value prior to the M9-class 2011 Tohoku and 2004 Sumatra quakes. *Geophysical Research Letters*, *39*(20). Retrieved from https://agupubs.onlinelibrary.wiley.com/doi/abs/10.1029/2012GL052997 doi: 10.1029/2012GL052997

Ogata, Y. (1985). Statistical models for earthquake occurrences and residual analysis for point processes. *Research Memo. Technical report Inst. Statist. Math., Tokyo.*, *288*.

Ogata, Y. (1988a). Space-time point-process models for earthquake occurrences. *Ann. Inst. Math.Statist.*, *50*, 379–402.

Ogata, Y. (1988b). Statistical models for earthquake occurrences and residual analysis for point processes. *J. Amer. Statist. Assoc.*, *83*, 9 – 27.

Ogata, Y. (1989). A monte carlo method for high dimensional integration. *Numerische Mathematik*, *55*(2), 137-157. Retrieved from http://dx.doi.org/10.1007/BF01406511 doi: 10.1007/BF01406511

Ogata, Y., & Katsura, K. (1993, 06). Analysis of temporal and spatial heterogeneity of magnitude frequency distribution inferred from earthquake catalogues. *Geophysical Journal International*, *113*(3), 727-738. Retrieved from https://doi.org/10.1111/j.1365-246X.1993.tb04663.x doi: 10.1111/j.1365-246X.1993.tb04663.x

Ogata, Y., & Katsura, K. (2006). Immediate and updated forecasting of aftershock hazard. *Geophysical Research Letters*, *33*(10). Retrieved from https://agupubs.onlinelibrary.wiley.com/doi/abs/10.1029/2006GL025888 doi: 10.1029/2006GL025888

Peng, Z., Vidale, J. E., Ishii, M., & Helmstetter, A. (2007). Seismicity rate immediately before and after main shock rupture from high-frequency waveforms in japan. *Journal of Geophysical Research: Solid Earth*, *112*(B3), n/a–n/a. Retrieved from http://dx.doi.org/10.1029/2006JB004386 (B03306) doi: 10.1029/2006JB004386

Petrillo, G., Landes, F., Lippiello, E., & Rosso, A. (2020). The influence of the brittle-ductile transition zone on aftershock and foreshock occurrence. *Nature Communications*, *11*, 3010. doi: 10.1038/s41467-020-16811-7

Petrillo, G., & Lippiello, E. (2020). Testing of the foreshock hypothesis within an epidemic like description of seismicity. *Geophysical Journal International*, *225*(2), 1236-1257. Retrieved from https://doi.org/10.1093/gji/ggaa611 doi: 10.1093/gji/ggaa611

Scholz, C. H. (1968). The frequency-magnitude relation of microfracturing in rock and its relation to earthquakes. *Bull. seism. Soc. Am.*, *58*, 399–415.

Scholz, C. H. (2015). On the stress dependence of the earthquake b value. *Geophysical Research Letters*, *42*(5), 1399-1402. Retrieved from https://agupubs.onlinelibrary.wiley.com/doi/abs/10.1002/2014GL062863 doi: 10.1002/2014GL062863

Schorlemmer, D., & Woessner, J. (2008). Probability of detecting an earthquake. *Bulletin of the Seismological Society of America*, *98*(5), 2103-2117. Retrieved from http://www.bssaonline.org/content/98/5/2103.abstract doi: 10.1785/0120070105

Shi, Y., & Bolt, B. A. (1982). The standard error of the magnitude-frequency b value. *Bulletin of the Seismological Society of America*, *72*(5), 1677-1687. Retrieved from http://www.bssaonline.org/content/72/5/1677.abstract

Tormann, T., Enescu, B., Woessner, J., & Wiemer, S. (2015). Randomness of megathrust earthquakes implied by rapid stress recovery after the Japan earthquake. *Nature Geoscience*, *8*, 152-158. doi: 10.1038/ngeo2343

Tormann, T., Wiemer, S., & Mignan, A. (2014). Systematic survey of high-resolution b value imaging along californian faults: Inference on asperities. *Journal of Geophysical Research: Solid Earth*, *119*(3), 2029-2054. Retrieved from https://agupubs.onlinelibrary.wiley.com/doi/abs/10.1002/2013JB010867 doi: https://doi.org/10.1002/2013JB010867

van der Elst, N. J. (2021). B-positive: A robust estimator of aftershock magnitude distribution in transiently incomplete catalogs. *Journal of Geophysical Research: Solid Earth*, *126*(2), e2020JB021027. Retrieved from https://agupubs.onlinelibrary.wiley.com/doi/abs/10.1029/2020JB021027 (e2020JB021027 2020JB021027) doi: https://doi.org/10.1029/2020JB021027

Wiemer, S., & Wyss, M. (1997). Mapping the frequency-magnitude distribution in asperities: An improved technique to calculate recurrence times? *J. Geophys. Res.*, *102*, 15,115-15,128.

Wiemer, S., & Wyss, M. (2002). Mapping spatial variability of the frequency-magnitude distribution of earthquakes. *Adv. Geophys.*, *45*, 259-302.

Wyss, M. (1973). Towards a physical understanding of the earthquake frequency distribution. *Geophysical Journal of the Royal Astronomical Society*, *31*(4), 341-359. Retrieved from https://onlinelibrary.wiley.com/doi/abs/10.1111/j.1365-246X.1973.tb06506.x doi: 10.1111/j.1365-246X.1973.tb06506.x

Figure 5.

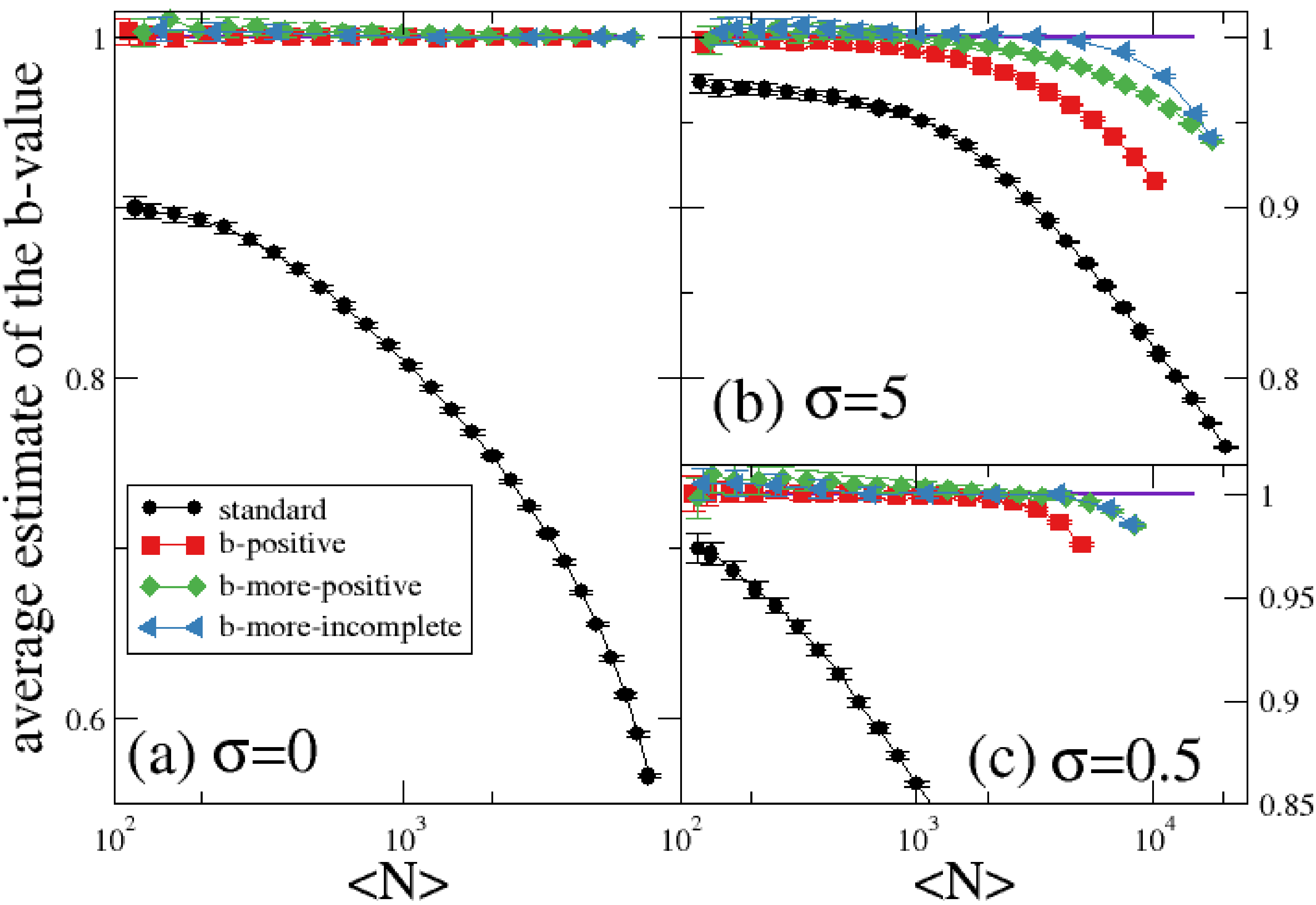

average estimate of the b-value
1
0.8
0.6
0.9
0.95
0.85
10^2
10^3
10^4
<N>
<N>
standard
b-positive
b-more-positive
b-more-incomplete
(a) σ=0
(b) σ=5
(c) σ=0.5

Figure 4.

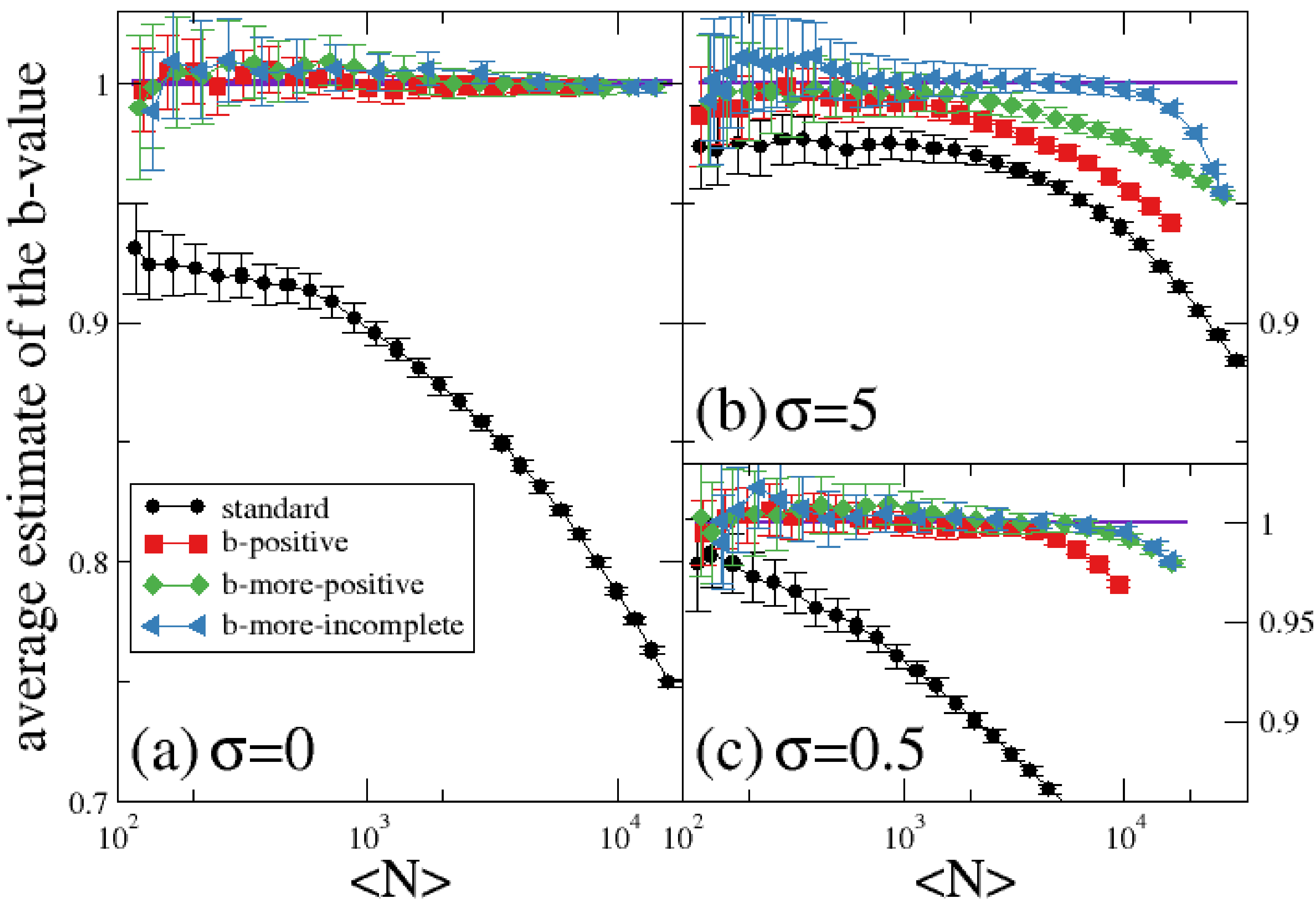

average estimate of the b-value
1
0.9
0.8
0.7
0.95
standard
b-positive
b-more-positive
b-more-incomplete
(a) σ=0
(b) σ=5
(c) σ=0.5
10^2
10^3
10^4
<N>

Figure 2.

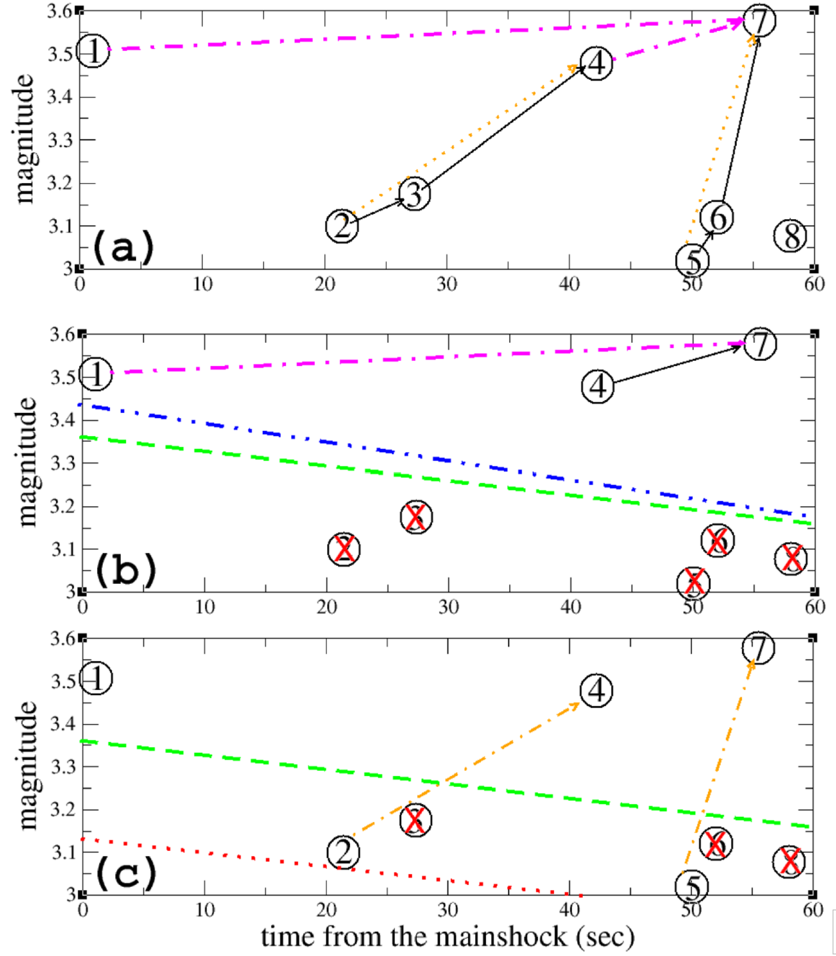

(a)
(b)
(c)
magnitude
time from the mainshock (sec)

Figure 1.

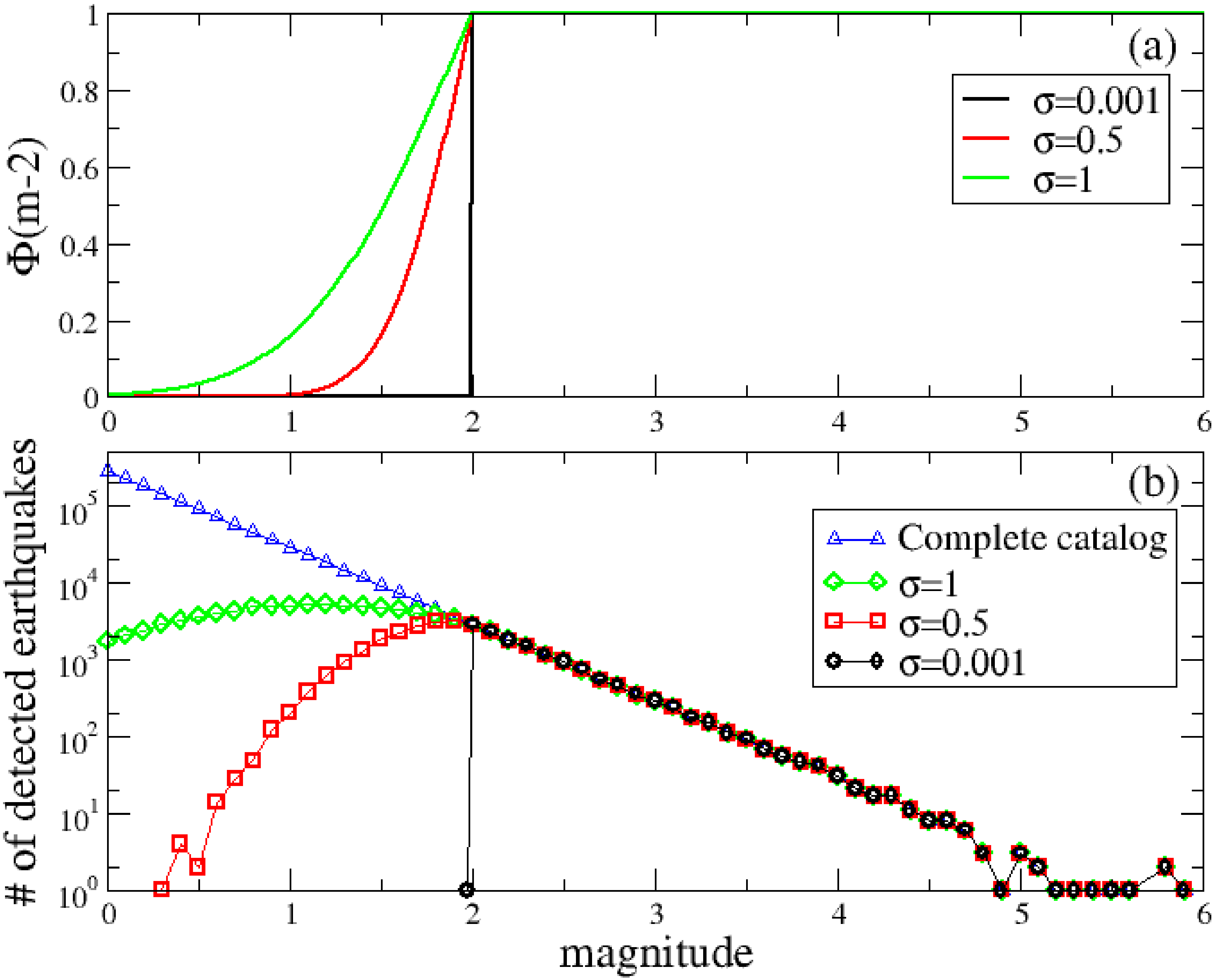

(a)
σ=0.001
σ=0.5
σ=1
Φ(m-2)
(b)
Complete catalog
σ=1
σ=0.5
σ=0.001
# of detected earthquakes
magnitude

Figure 3.

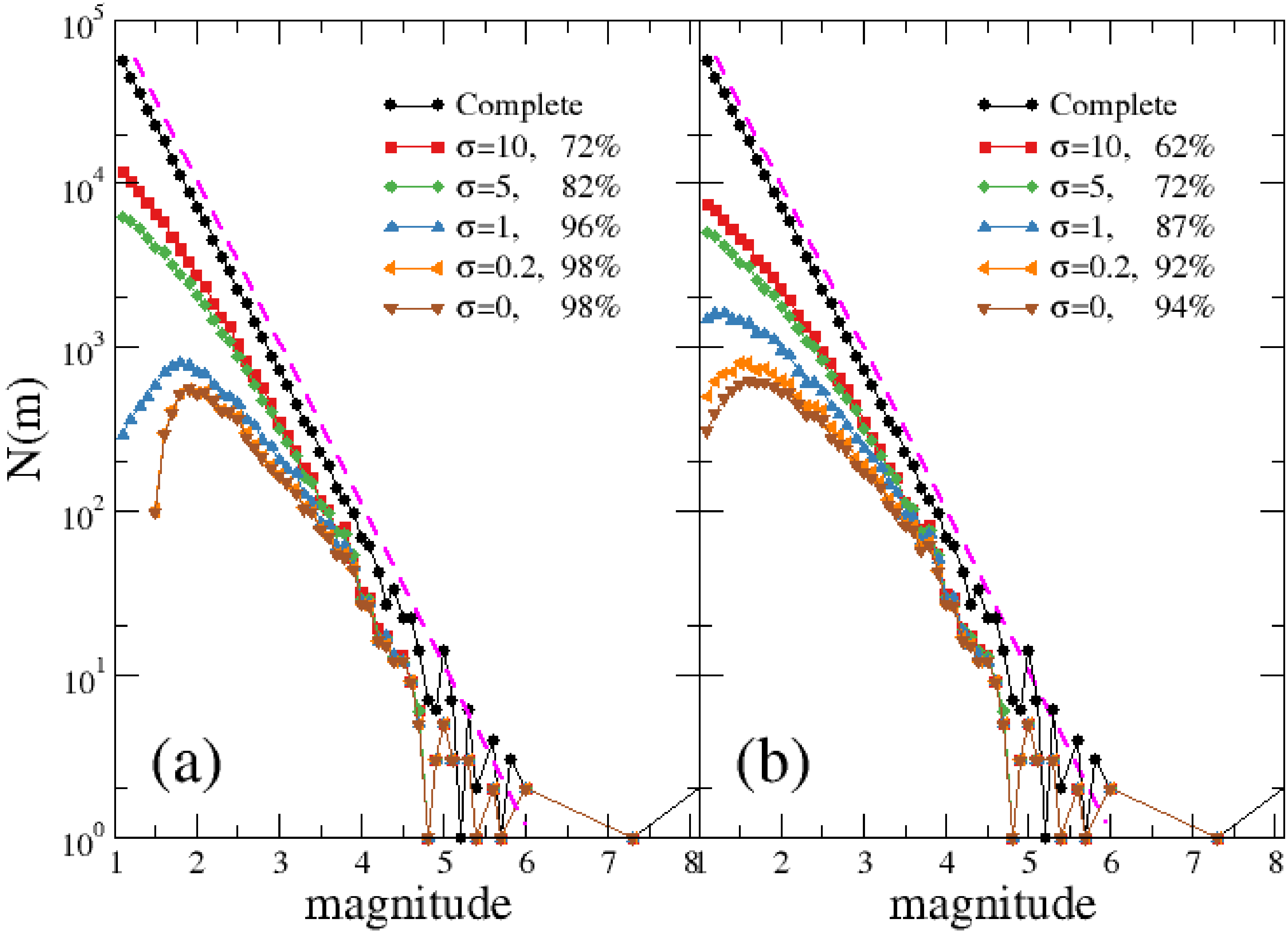
Complete
σ=10, 72%
σ=5, 82%
σ=1, 96%
σ=0.2, 98%
σ=0, 98%
Complete
σ=10, 62%
σ=5, 72%
σ=1, 87%
σ=0.2, 92%
σ=0, 94%
(a)
(b)
N(m)
magnitude
magnitude

Figure 6.

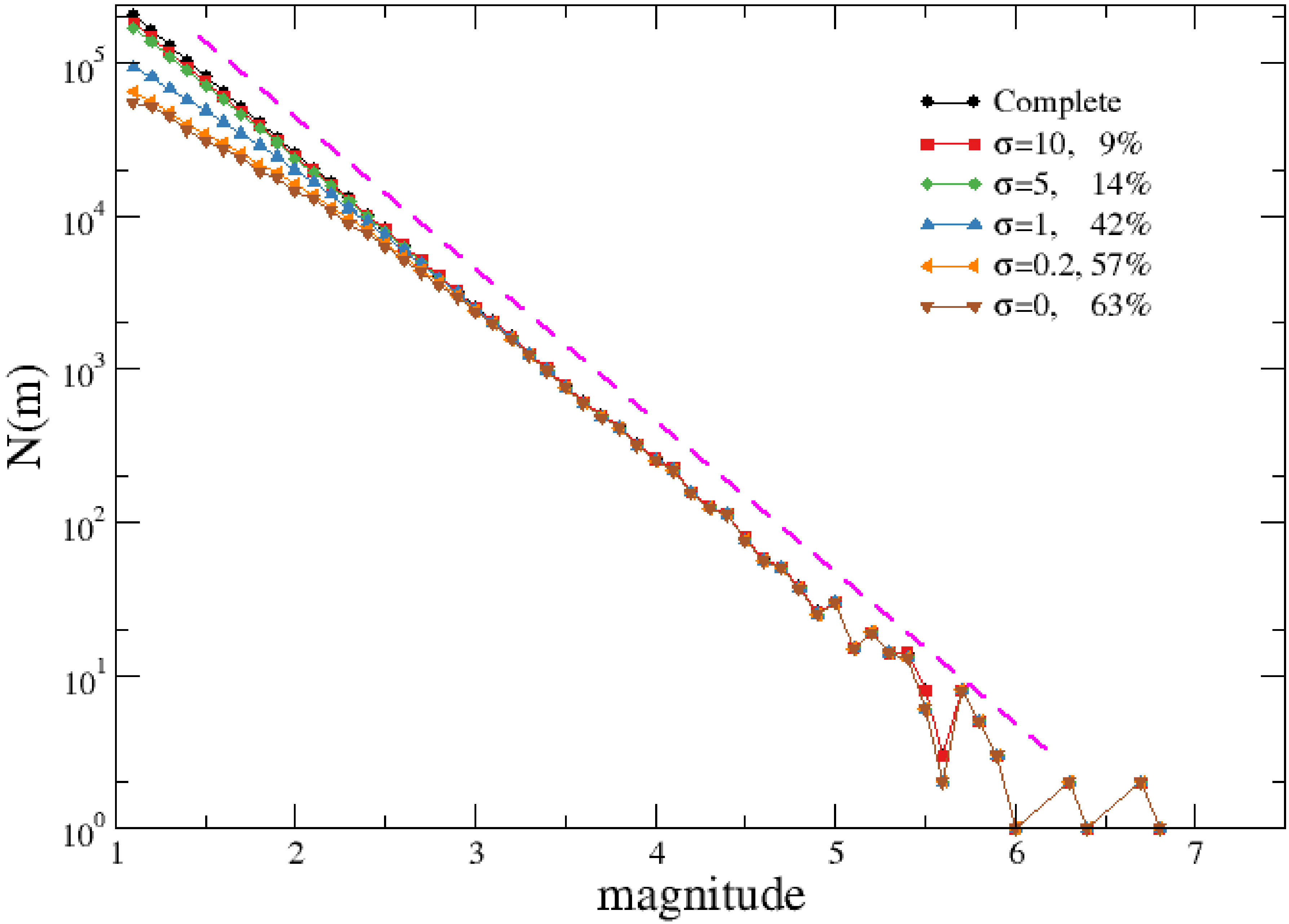

N(m)
magnitude
10^0
10^1
10^2
10^3
10^4
10^5
1
2
3
4
5
6
7
Complete
σ=10, 9%
σ=5, 14%
σ=1, 42%
σ=0.2, 57%
σ=0, 63%

Figure 7.

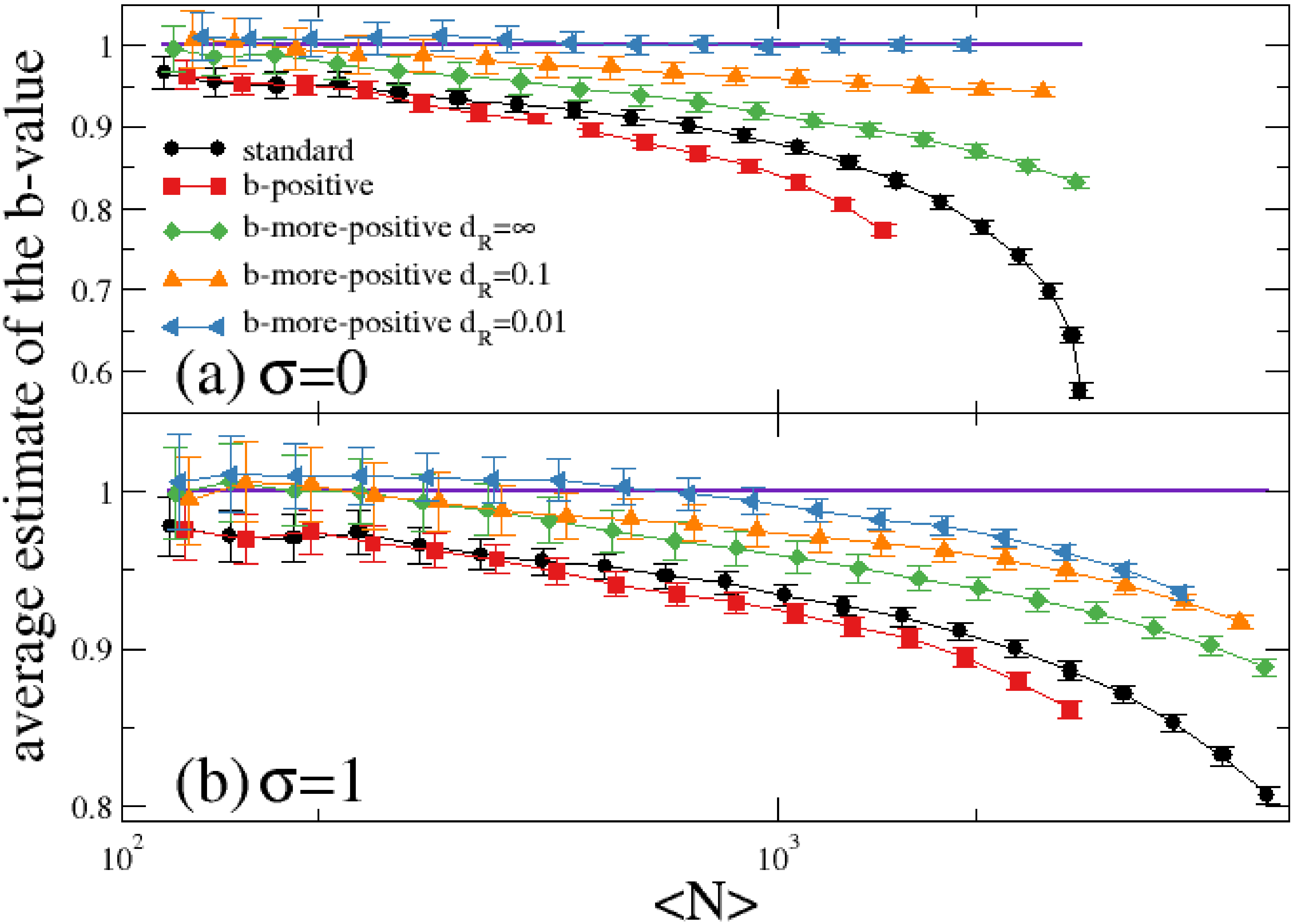

average estimate of the b-value
standard
b-positive
b-more-positive $d_R=\infty$
b-more-positive $d_R=0.1$
b-more-positive $d_R=0.01$
(a) $\sigma=0$
(b) $\sigma=1$
1
0.9
0.8
0.7
0.6
10^2
10^3
<N>

Figure 8.

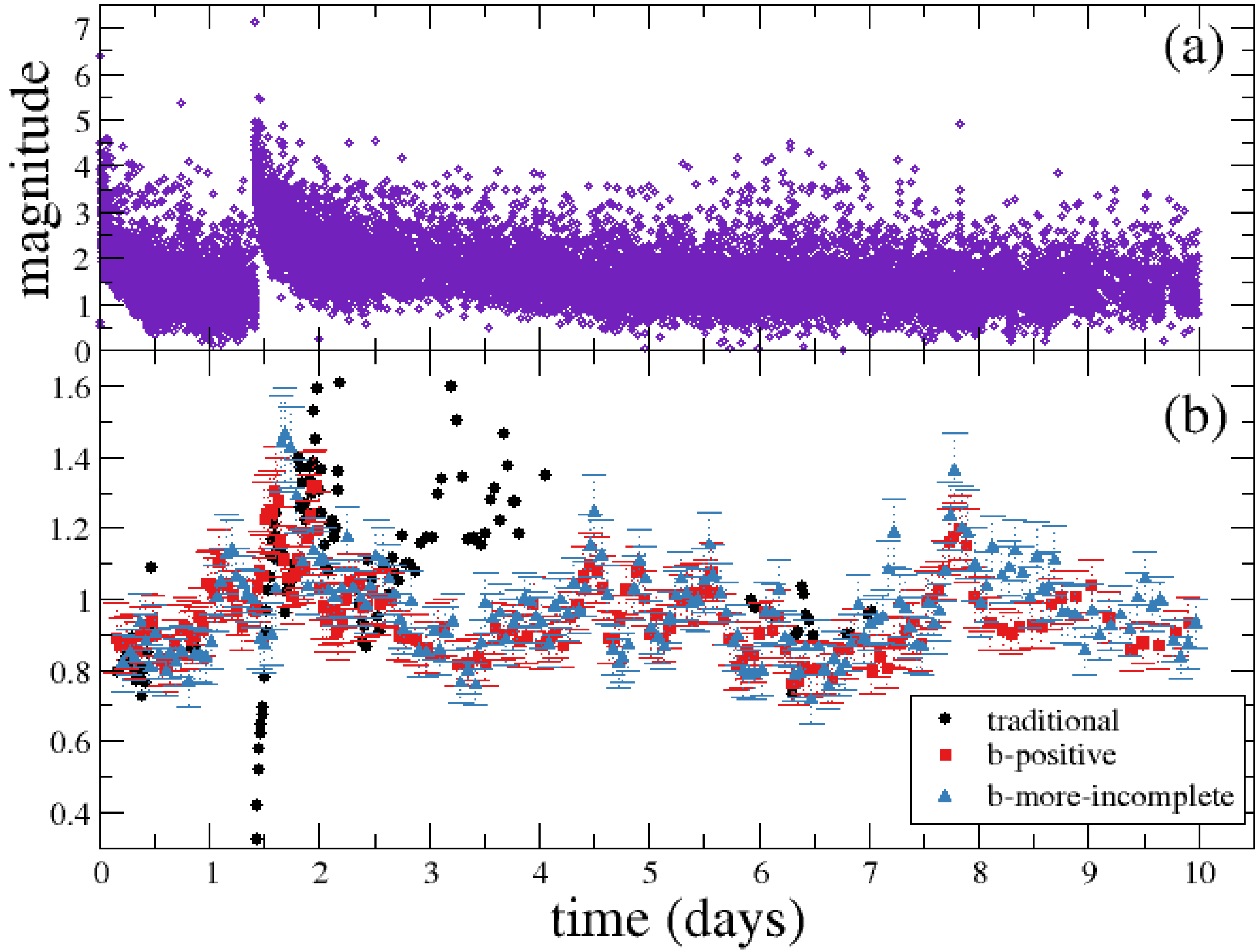

magnitude
(a)
(b)
traditional
b-positive
b-more-incomplete
time (days)

Figure 9.

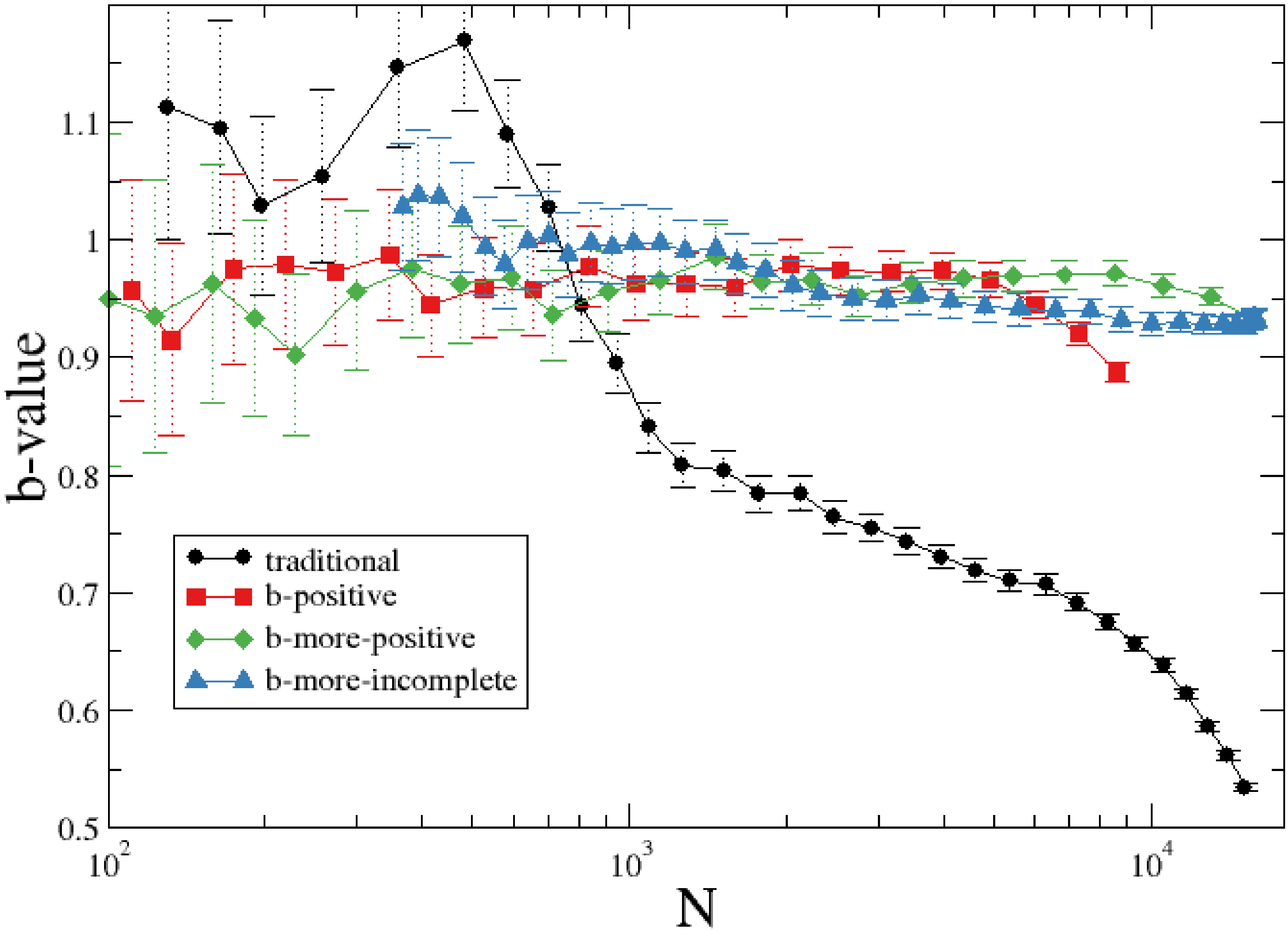

b-value
N
traditional
b-positive
b-more-positive
b-more-incomplete
1.1
1
0.9
0.8
0.7
0.6
0.5
10^2
10^3
10^4